2009

Modeling and Inference for Measured Crystal Orientations and a Tractable Class of Symmetric Distributions for Rotations in Three Dimensions

Melissa Ann Bingham
University of Wisconsin - La Crosse

Daniel J. Nordman
Iowa State University, dnordman@iastate.edu

Stephen B. Vardeman
Iowa State University, vardeman@iastate.edu

This is an Accepted Manuscript of an article published by Taylor & Francis in Journal of the American Statistical Association in 2009, available online: http://www.tandfonline.com/10.1198/jasa.2009.ap08741

Modeling and Inference for Measured Crystal Orientations and a Tractable Class of Symmetric Distributions for Rotations in 3 Dimensions

Melissa A. Bingham

Daniel J. Nordman

Stephen B. Vardeman

Iowa State University

Ames, IA, 50011

Author's Footnote

Melissa A. Bingham is a Ph.D. candidate, Daniel J. Nordman is Assistant Professor, and Stephen B. Vardeman is University Professor, Department of Statistics, Iowa State University, Ames, IA, 50011. This work is supported by NSF grant DMS #0502347 EMSW21-RTG awarded to the Department of Statistics, Iowa State University, and by the Ames Laboratory through U.S. Department of Justice COPS Program grant #2005CKWX0466 and interagency agreement #2002-LP-R-083 by the National Institute of Justice, through the Midwest Forensics Resource Center. The Ames Laboratory is operated for the U.S. Department of Energy by Iowa State University under contract #DE-AC02-07CH11358. The authors wish to thank Dr. Barbara Lograsso of Michigan Technological University for introducing us to the EBSD problem and Fran Laabs of Ames Laboratory, Iowa State University, for collecting the EBSD data. We further thank Iowa State University Professor Max Morris for an early suggestion that led us to identify and study the UARS class.

Abstract

Electron Backscatter Diffraction (EBSD) is a technique used in materials science to study the microtexture of metals, producing data which measure orientations of crystals in a specimen. We examine the precision of such data based on a useful class of distributions on orientations in 3 dimensions (as represented by 3×3 orthogonal matrices with positive determinant). While such modeling has received attention in the statistical literature, the approach taken has typically been from general "special manifold" considerations and the resulting methodology may not be easily accessible to non-specialists. We take a more direct modeling approach, beginning from a simple intuitively appealing mechanism for generating random orientations specifically in 3-space. The resulting class of distributions has many desirable properties, including directly interpretable parameters and relatively simple theory. We investigate the basic properties of the entire class and one-sample quasi-likelihood-based

inference for one member of the model class, producing new statistical methodology that proves practically useful in the analysis of EBSD data.

KEY WORDS: Directional data, Electron Backscatter Diffraction, Euler angles, Haar measure, von Mises distribution, orthogonal matrix, quasi-likelihood ratio test, UARS distribution, Wald test

1 Introduction

Our work is motivated by a materials science application that involves quantifying the precision of Electron Backscatter Diffraction (EBSD) data produced in studies of the microtexture of metals. Using a Scanning Electron Microscope (SEM), EBSD data result when a stationary beam of electrons is diffracted by atomic lattice planes in a target metal, creating an image called a Kikuchi diffraction pattern on a focal plane of sensors. These collected EBSD patterns are then matched to theoretical patterns based on the known crystal structure of the metal and machine geometry, which in turn indicates the orientation of cubic crystals in the metal (because different orientations produce angular differences in band location, band intensity, and band width in the diffraction pattern); see Randle (2003).

In the application motivating our work, a TSL MSC-2200 (EBSD) camera and Field Emission AmRay 1845 SEM are used along with OIM Version 4.2 Analytical Suite software to produce diffraction patterns and then fitted crystal orientations relative to some reference coordinate system (defined, for example, by the geometry of the machine or the macro geometry of a metal sample being studied) at points scanned on a 2-dimensional regular grid laid over a "flat" surface of a metal specimen. Data for two metals will be examined here. The first metal, high-iron-concentration nickel, was chosen for study because it produces ideal EBSD patterns. The nickel specimen had a surface area $40\mu\text{m} \times 40\mu\text{m}$ and the same region was scanned 14 times with at least 4000 measurements per run. Each observation represents the orientation of a cubic crystal at some scanned position on the metal surface

(and can be described by a 3×3 orthogonal rotation matrix). Seven scans taken on a fixed region of an aluminum sample will also be considered, although in less detail.

Since EBSD is a commonly used methodology, it is important to investigate the consistency of measurements it produces. Although the issue of EBSD measurement precision has received some attention in the materials science literature, methods of data collection and inference for experimental precision are not yet widely agreed upon. Often referenced as a source for EBSD precision, Demirel, El-Dasher, Adams, and Rollet (2000) examine variation in orientation measurements from a single scan on a silicon single crystal wafer in terms of the spread in "misorientation angles" between an unspecified reference coordinate system and measured crystal orientations. (For two orientations specified by 3×3 orthogonal rotation matrices $\mathbf{M}_1$ and $\mathbf{M}_2$, the misorientation axis and angle are such that when $\mathbf{M}_2$ is rotated around the misorientation axis by the (positive) misorientation angle, $\mathbf{M}_1$ results (see Randle, 2003, sec. 6.4.1).) The misorientation angles of Demirel et al. (2000) are then centered by subtraction of their mean, resulting in a spread of roughly -1° to 1°, and a "1°" precision is reported. A more natural analysis might be based on misorientation angles from a "central orientation." Wilson and Spanos (2001) used this kind of approach with observations from a single scan on a single crystal gallium arsenide sample and found misorientation angles from an orientation chosen to "minimize average misorientation" to be roughly between 0° and 1°. These authors then somewhat inexplicably report a "0.5°" precision based on these angles. In the event that measured orientations are fairly consistent and substantially different from the orientation of the reference coordinate system, the spread in absolute values of angles produced by the somewhat ad hoc methods of Demirel et al. (2000) can be expected to be roughly comparable to the spread in (inherently positive) misorientation angles produced using the more natural approach of Wilson and Spanos (2001). With that in mind, based on both the silicon work of Demirel et al. (2000) and the gallium arsenide study of Wilson and Spanos (2001), a "1° misorientation angle precision" is representative of the commonly held perception of EBSD in materials science.

The precision estimates available in the current literature are based on single scans of single crystals/grains (i.e. scans at neighboring locations on homogeneous specimens). Our intention here is to begin development of methods that will eventually allow us to coherently quantify multiple components of variation in more complicated cases, where multiple scans are taken on the same specimen and specimens are potentially composed of multiple crystals. Of first present interest is the basic single-site repeatability of data obtained through EBSD (a matter that seems to be thus far unaddressed in the materials science literature) — we wish to examine the variation in orientation measurements obtained when EBSD is used repeatedly at a single location on the same metal specimen. Then, quantifying the variation of measured orientations thought to be from within a single grain (in the style of existing work) is a second problem of subject matter interest. Probability models for rotation matrices are potentially useful for describing the variation in scanning results and quantifying the nature of within-grain variation.

In the statistical literature, the most commonly referenced distribution for rotation matrices is the matrix (von Mises) Fisher distribution (sometimes referred to as the Langevin distribution) introduced by Downs (1972). Important advances have since been made by Khatri and Mardia (1977) and Jupp and Mardia (1979), with further work done by Prentice (1986), Mardia and Jupp (1999), Rancourt, Rivest, and Asselin (2000), Chikuse (2003), and Rivest, Baillargeon, and Pierrynowski (2008). But practical limitations remain. Parameters of the distribution are not easily interpreted, inference is not simple, and simulation from this distribution is not obvious. These considerations motivate León, Massé, and Rivest (2006) to introduce the so-called Cayley distributions. Although the Cayley distributions provide improvements over the matrix Fisher distribution in these areas, some of these problems (particularly of interpretability of parameters and ease of use of existing methodology) remain substantial. What is more, much of the EBSD data we have seen are not well-described by these existing models. We have therefore found it useful to abstract a property known to be shared by many symmetric distributions on 3-dimensional orientations and to use this as

the basis for defining a very broad class of models for rotation matrices with

i) an intuitively appealing constructive definition, and

ii) directly interpretable parameters

that facilitates the development and application of statistical methods. Here we will provide some general development and show how a newly identified element of this model class can be used to address the instrument repeatability problem in materials science.

The following is a loose initial description of the modeling idea for rotation matrices (more geometric details can be found in Section 2.1). For Ω the set of 3×3 orthogonal matrices with positive determinant (and that thus preserve the right hand rule) and $\mathbf{S} \in \Omega$ representing some central location or principal direction, view a random orientation $\mathbf{O} \in \Omega$ as of the form $\mathbf{O} = \mathbf{SM}$ for a random perturbation $\mathbf{M} \in \Omega$ of the 3×3 identity matrix. As it turns out, for the basic symmetric matrix Fisher and Cayley distributions for $\mathbf{O}$, the matrix $\mathbf{M} \equiv M(\mathbf{U}, r)$ can be thought of as arising from a random rotation of the 3-dimensional axes through angle $r \in (-\pi, \pi]$ about a random axis prescribed by unit vector $\mathbf{U}$ uniformly distributed over the unit sphere in 3-space. The variable $|r|$ corresponds to the materials science literature's "misorientation angle" between $\mathbf{S}$ and $\mathbf{O}$ (see Randle, 2003). The angle r is distributed independently of the random axis and has a marginal distribution symmetric on $(-\pi, \pi]$ which is indirectly and restrictively inherited from the matrix Fisher or Cayley model directly specified for $\mathbf{O}$ (see León et al., 2006, sec. 5.2). It seems however, that more flexible modeling of orientation data might grow out of allowing other distributions for the angle r.

Figure 1 is a plot of theoretical quantiles for the distribution of $|r|$ versus empirical $|\hat{r}|$ quantiles after fitting the matrix Fisher and Cayley models to a small sample of EBSD data representing multiple measurements at the same location on the nickel specimen. Figure 1 suggests that the fits to the distributions from the existing literature are not good and that other forms for the distribution of r might profitably be explored. For example, by selecting a von Mises circular distribution for r (symmetric about 0) and plotting resulting quantiles

of $|r|$ versus empirical quantiles of $|\hat{r}|$ for the same data represented in Figure 1, one obtains the substantially more pleasant Figure 2.

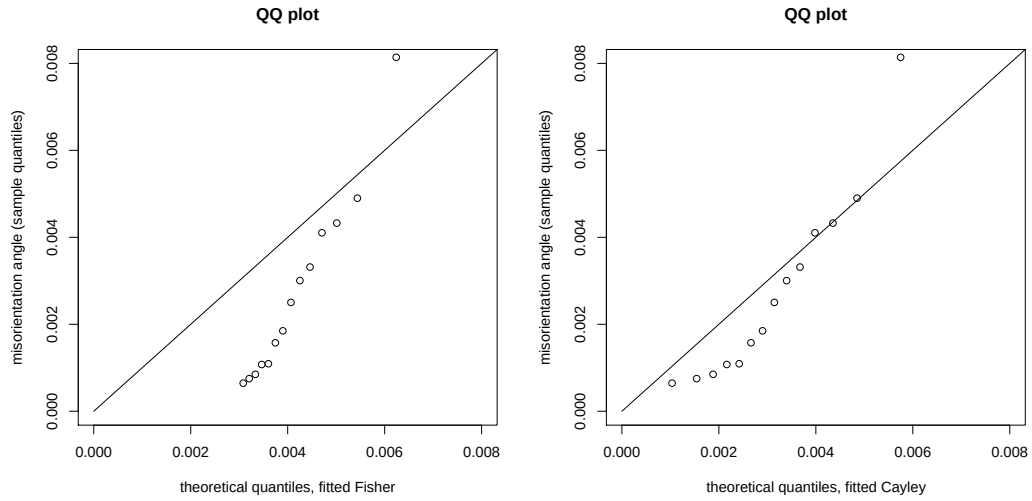

Figure 1: Q-Q plots for the fitted misorientation angles obtained from fourteen repeat EBSD observations, using the matrix Fisher (left) and Cayley (right) models on Ω

In this paper, we consider two small data sets representing a part of the nickel EBSD data. The first consists of the fourteen repeat measurements from one location on the scans represented in Figures 1 and 2 and will be used to study the repeatability of the EBSD data. The second data set, consisting of measurements for 70 different locations on a single scan that all appeared to be within the same grain, will be used to study the within grain variation. Table 1 presents the fourteen repeat measurements, represented in Euler angle form. (For more on the Euler angle representation of a 3×3 orthogonal rotation matrix, see Section 3.1.) In Section 5, two small data sets from the aluminum scans will also be considered. Seven repeat measurements from the same location on the scans and 50 locations appearing to be within a single grain on one scan will be considered.

To be more precise about what is presented in Figures 1 and 2 and to prepare for a parallel treatment of the second nickel data set, we begin by defining an estimate of the principal orientation $\mathbf{S}$ for a sample. Suppose that $\bar{\mathbf{o}} = \sum_{i=1}^{n} \mathbf{o}_i/n$ for data orientations $\mathbf{o}_1, \ldots, \mathbf{o}_n \in \Omega$.

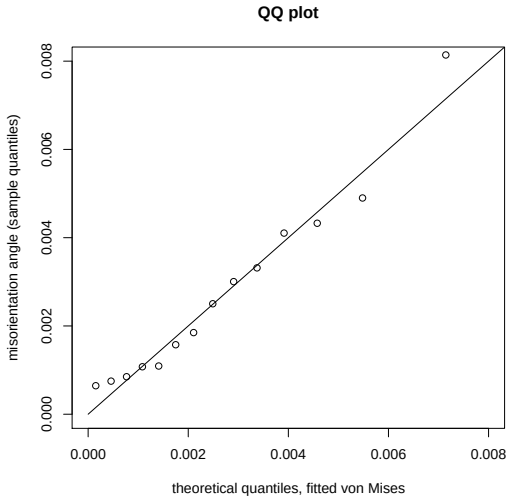

Figure 2: Q-Q plot for the fitted misorientation angles obtained from fourteen repeat EBSD observations, using the von Mises circular distribution on r

Table 1: Repeat EBSD data for a single location on a nickel specimen (in Euler angle form)

Observation	α	β	γ
1	5.857001	0.9280639	4.220050
2	5.862054	0.9357848	4.216083
3	5.861929	0.9377740	4.219057
4	5.864537	0.9373403	4.215629
5	5.861906	0.9340686	4.217158
6	5.861424	0.9357253	4.217151
7	5.862159	0.9369018	4.215104
8	5.866320	0.9340180	4.216715
9	5.861765	0.9358679	4.216700
10	5.856148	0.9347951	4.221809
11	5.866616	0.9342294	4.212785
12	5.860286	0.9363732	4.217755
13	5.862718	0.9353843	4.216685
14	5.862907	0.9358418	4.215240

The value of $\mathbf{S}$ that maximizes $tr(\mathbf{S}^T\bar{\mathbf{o}})$ (for $tr(\mathbf{A})$ the trace of $\mathbf{A}$) is commonly used as an estimate for $\mathbf{S}$. It is the moment estimator for the modal rotation of the Cayley distribution in 3 dimensions (León et al., 2006, p. 421), and is the mean direction for the matrix Fisher distribution in 3 dimensions (Khatri and Mardia, 1977, p. 96).

Once $\mathbf{S}$ has been estimated, we find the misorientation angle $|r|$ required to obtain each observation from the fitted $\mathbf{S}$. We can then fit a choice of circular distribution for $r \in (-\pi, \pi]$ to the sample misorientation angles using maximum likelihood. For each data set, the von Mises circular distribution (see Mardia and Jupp, 2000) and the distributions on r that give the Cayley and symmetric matrix Fisher distributions were fit. Figures 1 and 2 gave the sample quantiles plotted against the theoretical quantiles for the first nickel data set (repeat scans at a single location). Figure 3 contrasts the fits for the between-location data.

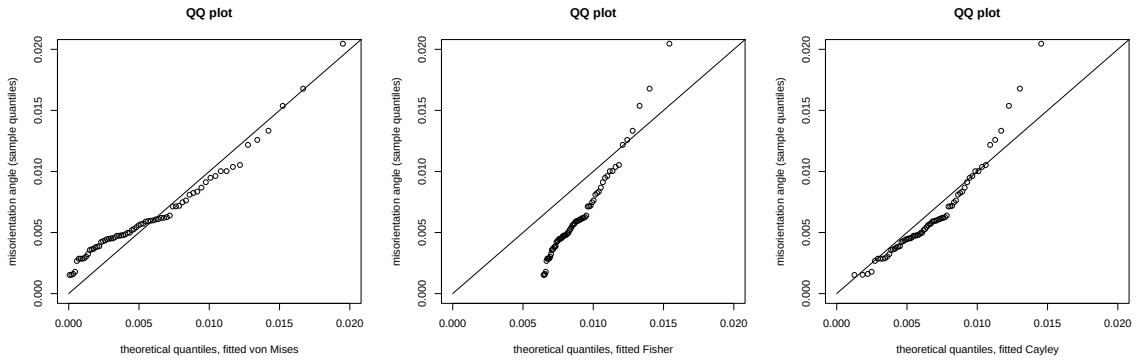

(a) (b) (c)

Figure 3: Q-Q plots for the misorientation angles $|r|$ obtained from the 70 observations within a single grain of the nickel specimen, for fitted (a) von Mises (b) matrix Fisher and (c) Cayley distributions

The EBSD nickel data sets show that there are cases where previously developed models are not appropriate and that there is a need for greater flexibility in modeling 3-dimensional rotations. In the next section, we more formally develop what we will call the UARS class of distributions introduced above. Most existing work in this area begins by defining distributions on somewhat abstract "special manifolds" and develops results for 3-dimensional

rotations as special cases. Our approach is more direct. We begin from a very concrete and easily described mechanism specifically for generating random rotations in 3-space. After defining the UARS class of distributions, we examine its properties and those of quasi-likelihood-based inference for one member of the model class, where the angle r is assumed to follow a von Mises circular distribution. We then apply our results to the EBSD data. In addition to the nickel data (Figures 2 and 3), the von Mises circular distribution also adequately describes the misorientation angles obtained from two small aluminum data sets; see the supplementary on-line Appendix for Q-Q plots.

2 Uniform-Axis-Random-Spin distributions

2.1 A concrete model for the generation of 3-dimensional orientation data

To study the variation in a set of "measurements" belonging to Ω, we begin by supposing that $\mathbf{o}_i \in \Omega$ for $i = 1, \ldots, n$ are data like those giving fitted orientations of cubic crystals known to share a common principal orientation $\mathbf{S} \in \Omega$. We wish to model the deviations of $\mathbf{o}_1, \mathbf{o}_2, \ldots, \mathbf{o}_n$ from $\mathbf{S}$.

We begin with a physical description of a model of data generation for the case $\mathbf{S} = \mathbf{I}_{3\times 3}$ (the 3×3 identity matrix). To create a random rotation $\mathbf{O} \in \Omega$ we first generate a point uniformly on the unit sphere. We can represent this point in terms of polar coordinates $\theta \in [0, \pi]$ and $\phi \in [0, 2\pi]$ as the unit vector

$$\mathbf{U} = (u, v, w)^T = (\sin\theta\cos\phi, \sin\theta\sin\phi, \cos\theta)^T. \tag{1}$$

Secondly, we independently generate an angle $r \in (-\pi, \pi]$ from a circular distribution symmetric about 0. In order to allow the spread of this circular distribution to depend on a parameter, we will write $r \sim \text{Circ}(\kappa)$, where the $\text{Circ}(\kappa)$ distribution has density $C(r|\kappa)$. The last step is to rotate all of 3-space (including the unit sphere and the vectors $(1, 0, 0)$, $(0, 1, 0)$, and $(0, 0, 1)$ specifying the original coordinate axes) about the vector in (1) by the

angle r, giving $\mathbf{O} \in \Omega$ with columns that specify the rotated locations of $(1,0,0)$, $(0,1,0)$, and $(0,0,1)$ respectively.

An observation $\mathbf{O}$ generated as above can be expressed in terms of the elements of $\mathbf{U}$ in (1) and r as $\mathbf{O} = M(\mathbf{U}, r)$, where

$$M(\mathbf{U}, r) \equiv \mathbf{U}\mathbf{U}^T + (\mathbf{I}_{3\times 3} - \mathbf{U}\mathbf{U}^T)\cos r + \begin{pmatrix} 0 & -u_3 & u_2 \\ u_3 & 0 & -u_1 \\ -u_2 & u_1 & 0 \end{pmatrix} \sin r. \tag{2}$$

In this model, small $|r|$ produces an observation $\mathbf{O}$ that differs less from $\mathbf{I}_{3\times 3}$ than will one with large $|r|$. (For example, consider the extreme case $r = 0$ which will produce an observation $\mathbf{O} = \mathbf{I}_{3\times 3}$ regardless of $\mathbf{U}$.) Therefore, the parameter κ of the circular distribution governs the "spread" of orientation data generated according to this model. So we will say that for $\mathbf{U}$ uniform on the sphere independent of $r \sim \text{Circ}(\kappa)$, $\mathbf{O}$ as in (2) has a Uniform-Axis-Random-Spin distribution with parameters $\mathbf{I}_{3\times 3}$ and κ, i.e. $\mathbf{O} \sim \text{UARS}(\mathbf{I}_{3\times 3}, \kappa)$.

Such distributions for $\mathbf{O}$ can alternatively be expressed in terms of quaternions. If $\mathbf{x} = (x_1, x_2, x_3, x_4) \in \mathbb{R}^4$ is a unit vector, then there is a mapping $\mu : \mathbb{R}^4 \to \Omega$ with $\mathbf{O} = \mu(\mathbf{x})$ such that there is a one-to-one correspondence between $\mathbf{O}$ and $\pm\mathbf{x}$; see Prentice (1986) who uses axial distributions on the quaternions to define distributions on Ω. The quaternion representation of $\mathbf{O}$ as in (2) is $\mathbf{x} = (\sin(r/2)u,\ \sin(r/2)v,\ \sin(r/2)w,\ \cos(r/2))$. In this form, a rotationally symmetric distribution for $\mathbf{x}$ about the axis $(0,0,0,1)$, as defined by Watson (1983, sec. 3.4), is possible through a distribution on $\cos(r/2)$. The UARS distributions can thus also be viewed as a family of rotationally symmetric distributions on the quaternions. While this representation in terms of quaternions is elegant, we have not found it to simplify any of our analyses. The rotation-axis-and-angle motivation and representation that we use here both has an appealing concrete interpretation and leads to easily understood and effective calculations. Further, the concept of a misorientation angle $|r|$ and misorientation axis $\mathbf{U}$ is familiar to materials scientists and thus has a connection to our motivating application.

A UARS($\mathbf{I}_{3\times 3}$, κ) distribution describes "directionally symmetric" perturbations of $\mathbf{I}_{3\times 3}$.

Consider now modeling directionally symmetric perturbations of some other orientation, described by the orthogonal matrix $\mathbf{S}$. (This will allow modeling of measured crystal orientations where the true orientation is $\mathbf{S}$, described by a principal orientation of the distribution at $\mathbf{S}$.) With $\mathbf{U}$ uniform on the sphere independent of $r \sim \text{Circ}(\kappa)$ the distribution of

$$\mathbf{O} = \mathbf{S} \cdot M(\mathbf{U}, r) \tag{3}$$

has principal direction at $\mathbf{S}$. We will call the distribution of $\mathbf{O}$ constructed as in (3) a Uniform-Axis-Random-Spin distribution with parameters $\mathbf{S} \in \Omega$ and κ and write $\mathbf{O} \sim \text{UARS}(\mathbf{S}, \kappa)$. This two-component parameterization is natural and useful in interpreting the effects of variability specified by κ and central location at $\mathbf{S}$ in modeling. We have also enumerated some nice probabilistic (symmetry) properties of these models in the Appendix, such as the fact that (3) is distributionally equivalent to the definition $\mathbf{O} = M(\mathbf{U}, r) \cdot \mathbf{S}$.

As mentioned in Section 1, distributions for matrix data studied in the existing literature, like the Fisher and Cayley distributions, have often grown out of density derivations beginning with manifolds (see Khatri and Mardia, 1977), and specializing these calculations to rotation matrices often yields a characterization in terms of an independent pair $(\mathbf{U}, r)$ where r is forced to have a particular distributional form. In this sense, distributions on rotation matrices defined in terms of an axis and spin are not unique to the present work. Our point here is that we have found *beginning* from this constructive definition made especially for 3-dimensional rotations, where one may freely model the r-spin distribution, to be an intuitively appealing, tractable and highly effective approach to modeling and statistical inference.

2.2 The UARS(S, κ) density

In the modeling construction above, the first step requires specifying a density $C(r|\kappa)$ for $r \in (-\pi, \pi]$, symmetric about 0 and having concentration parameter κ. It then follows that a matrix density for $\mathbf{O} \sim \text{UARS}(\mathbf{S}, \kappa)$, with respect to the Haar measure which acts as a

"uniform distribution" on the collection Ω of rotation matrices, is given by

$$f(\mathbf{o}|\mathbf{S},\kappa) = \frac{4\pi}{3 - tr(\mathbf{S}^T\mathbf{o})} C\left(\arccos[2^{-1}(tr(\mathbf{S}^T\mathbf{o}) - 1)]\Big|\kappa\right), \quad \mathbf{o} \in \Omega. \tag{4}$$

See the supplementary on-line Appendix for details on the derivation of this density.

The UARS class of distributions allows unrestricted choice of distribution for r (or $|r|$). But unless the function $\dfrac{C(r|\kappa)}{1-\cos r}$ has a finite limit at $r = 0$, the density (4) will be unbounded at $\mathbf{o} = \mathbf{S}$. Thus, some of the natural choices for the distribution on r, such as the von Mises circular distribution explored next, result in densities with singularities at $\mathbf{S}$. Other choices for the distribution on r that are perhaps less natural, but result in bounded matrix densities (4) are the "scaled" Beta(3, κ) distribution and the truncated Maxwell-Boltzmann distribution. The Haar measure itself corresponds to a Lebesgue density for r of $(1 - \cos|r|)/\pi$, $r \in (-\pi, \pi]$ (Miles, 1965), for which (4) is bounded. León et al. (2006, sec. 5.2) give the density for r corresponding to the Cayley distribution (introduced in the same paper) and for the symmetric matrix Fisher distribution (introduced by Downs (1972)), for which (4) is again bounded.

For modeling the EBSD data, we consider UARS($\mathbf{S}$, κ) matrix models where r has a von Mises circular density given by

$$C(r|\kappa) = [2\pi I_0(\kappa)]^{-1} \exp[\kappa\cos(r)], \; r \in (-\pi, \pi] \tag{5}$$

where $I_0(\kappa) = (2\pi)^{-1} \displaystyle\int_{-\pi}^{\pi} \exp[\kappa\cos(r)]\, dr$ is the modified Bessel function of order zero. This density is unimodal, symmetric about 0, and as $\kappa \to \infty$, the distribution becomes approximately Normal with mean 0 and variance $\frac{1}{\kappa}$. For more on the von Mises distribution see Mardia and Jupp (2000).

Though the von Mises version of (4) given by

$$f(\mathbf{o}|\mathbf{S},\kappa) = \frac{2}{3 - tr(\mathbf{S}^T\mathbf{o})} [I_0(\kappa)]^{-1} \exp\left[\frac{\kappa}{2}(tr(\mathbf{S}^T\mathbf{o}) - 1)\right], \quad \mathbf{o} \in \Omega, \tag{6}$$

is unbounded, the choice of von Mises as a circular distribution for r is a natural one (and appropriately describes our crystallographic data as seen in Figures 2 and 3). We denote the von Mises version of the UARS($\mathbf{S}$, κ) distribution by vM-UARS($\mathbf{S}$, κ).

Because the density (6) gives an unbounded likelihood, in Section 3.2 we will discuss a type of quasi-likelihood inference for the vM-UARS distributions. The quasi-likelihood we will use results from treating

$$f(\mathbf{o}|\mathbf{S},\kappa) = [I_0(\kappa)]^{-1} \exp\left[\frac{\kappa}{2}(tr(\mathbf{S}^T\mathbf{o}) - 1)\right], \quad \mathbf{o} \in \Omega, \tag{7}$$

as a "quasi-density" on Ω in replacement of (6). Notice that (7) is not the symmetric matrix Fisher density for $\mathbf{O}$ by virtue of the fact that it is not properly normalized. (The Fisher density for $\mathbf{O}$ corresponds to (4) with a density $C(r|\kappa)$ given by multiplying the circular von Mises density (5) with concentration parameter 2κ by $1 - \cos r$ and normalizing.)

To get some idea of what the vM-UARS($\mathbf{S}$, κ) distribution is like, Figures 4 and 5 illustrate the vM-UARS($\mathbf{I}_{3\times3}$, κ) distributions with κ values of 5 and 10. In Figure 4 the contours shown on the spheres outline regions enclosing increasing amounts of probability associated with the placement of the (randomly) rotated coordinate axes for the two vM-UARS($\mathbf{I}_{3\times3}$, κ) distributions. If the contour closest to each axis is considered the first contour, then $(10\times i)\%$ of realizations keep all 3 perpendicular axes within the region represented by the i^{th} contours about x, y, and z (simultaneously). As κ increases, probability accumulates more quickly as we move away from the principal direction $\mathbf{S} = \mathbf{I}_{3\times3}$. (If we had attempted to picture distributions with small κ, regions of high probability for the different axes would have seen significant overlap.) In Figure 5 each set of 3 perpendicular axes represents one orientation generated from the vM-UARS($\mathbf{I}_{3\times3}$, κ) distribution. As κ increases, the orientations become less spread about the principal direction (represented by the axes at x, y, and z).

The value κ controls the spread of the misorientation angle $|r|$ between $\mathbf{S}$ and what is observed, and thus the corresponding "spread" of the vM-UARS($\mathbf{S}$, κ) distribution. Let $\Delta_1(\kappa)$ be the median of the distribution of $|r|$ so that $(-\Delta_1(\kappa), \Delta_1(\kappa))$ captures 50% of the von Mises(κ) probability. Then let $\Delta_2(\kappa)$ be the median of the distribution of the maximum angle between an $\mathbf{S}$-rotated and a vM-UARS($\mathbf{S}$, κ)-rotated coordinate axis. Table 2 illustrates the relationship between $\Delta_1(\kappa)$ and $\Delta_2(\kappa)$ for various choices of κ. The values of

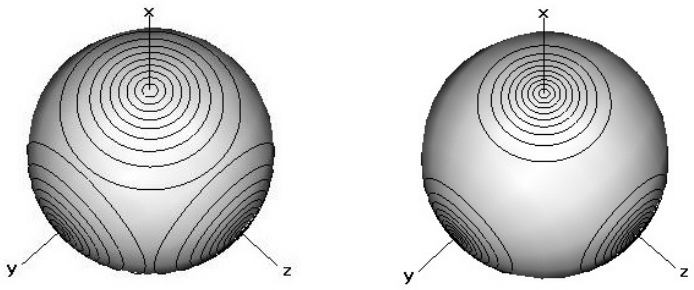

Figure 4: Probability content contours for vM-UARS distributions with $\kappa = 5$ (left) and 10 (right) (the axes shown are those represented by principal direction $\mathbf{S}$)

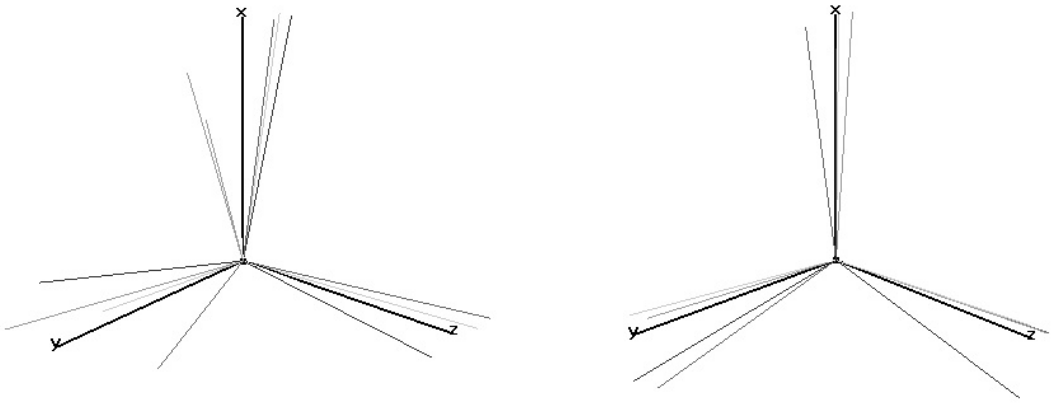

Figure 5: Five random orientations generated from vM-UARS distributions with $\kappa = 5$ (left) and 10 (right) (the axes at x, y, and z are those represented by principal direction $\mathbf{S}$)

$\Delta_1(\kappa)$ were computed using numerical integration and each value of $\Delta_2(\kappa)$ presented is based on a sample of 100,000 vM-UARS realizations. Obviously, there is a close correspondence between $\Delta_1(\kappa)$ and $\Delta_2(\kappa)$, and κ directly controls the concentrations of the von Mises and vM-UARS distributions. ($\Delta_2(\kappa)$ is slightly smaller than $\Delta_1(\kappa)$ as the maximum rotation of a coordinate axis is for each realization no more than the misorientation angle between the realization and $\mathbf{S}$.)

Table 2: Values of the medians $\Delta_1(\kappa)$ and $\Delta_2(\kappa)$ for various choices of κ

κ	$\Delta_1(\kappa)$	$\Delta_2(\kappa)$
1	0.80977	0.77526
5	0.31170	0.30218
10	0.21657	0.20923
20	0.15194	0.14697
50	0.09567	0.09232
100	0.06755	0.06519
500	0.03017	0.02909

3 One-sample quasi-likelihood and inference for the von Mises version of the UARS distributions

3.1 Parameterization of S

In what follows it will be useful to parameterize the principal direction $\mathbf{S} = g(\alpha, \beta, \gamma)$ as a function of Euler angles $\alpha \in [0, 2\pi]$, $\beta \in [0, \pi]$, and $\gamma \in [0, 2\pi]$. (The Euler angle parameterization of a rotation matrix is familiar to material scientists and when using EBSD, the orientations are typically output in Euler angle form; additionally, the parameterization also allows simple evaluation of a quasi-likelihood function.) Euler angles can be used to specify the orientation of an object in 3-dimensional Euclidean space relative to some reference coordinate system by subjecting the object to a sequence of three rotations, which are, in order,

1) a (counterclockwise) rotation of α radians about the z-axis at $(0, 0, 1)$,

2) a (counterclockwise) rotation of β radians about the x-axis at $(1, 0, 0)$, and

3) a (counterclockwise) rotation of γ radians again about the z-axis.

(Other orders and choices of axes are obviously possible.) Each of these rotations can describe a 3×3 rotation matrix $\mathbf{S} = g(\alpha, \beta, \gamma)$, where $g : [0, 2\pi] \times [0, \pi] \times [0, 2\pi] \to \Omega$ is defined by

$$
\begin{aligned}
g(\alpha, \beta, \gamma) &= \begin{pmatrix} \cos\gamma & \sin\gamma & 0 \\ -\sin\gamma & \cos\gamma & 0 \\ 0 & 0 & 1 \end{pmatrix} \begin{pmatrix} 1 & 0 & 0 \\ 0 & \cos\beta & \sin\beta \\ 0 & -\sin\beta & \cos\beta \end{pmatrix} \begin{pmatrix} \cos\alpha & \sin\alpha & 0 \\ -\sin\alpha & \cos\alpha & 0 \\ 0 & 0 & 1 \end{pmatrix} \\
&= \begin{pmatrix} \cos\alpha\cos\gamma - \sin\alpha\sin\gamma\cos\beta & \sin\alpha\cos\gamma + \cos\alpha\sin\gamma\cos\beta & \sin\gamma\sin\beta \\ -\cos\alpha\sin\gamma - \sin\alpha\cos\gamma\cos\beta & -\sin\alpha\sin\gamma + \cos\alpha\cos\gamma\cos\beta & \cos\gamma\sin\beta \\ \sin\alpha\sin\beta & -\cos\alpha\sin\beta & \cos\beta \end{pmatrix}.
\end{aligned} \tag{8}
$$

The function g is onto Ω and is one-to-one except in cases where $\beta = 0$ or $\beta = \pi$ (see Morawiec, 2004). So strictly speaking, g is not invertible. But in what follows we will treat it as if it were. Nearly all elements of Ω have unique representations in terms of the three Euler angles just introduced, and it is the elements of Ω that are fundamental (as opposed to the three angles used here). In a rare case where an orientation $\mathbf{S}$ is needed without a unique representation in Euler angles, we may rotate all observations by an arbitrary rotation matrix $\mathbf{R}$ (e.g., a counterclockwise rotation by $\frac{\pi}{2}$ radians about $(1, 0, 0)$) and do inference for the UARS($\mathbf{RS}$, κ) distribution. Estimates and confidence regions for $\mathbf{RS}$ can be obtained and then rotated by $\mathbf{R}^T$ to give estimates and confidence regions for $\mathbf{S}$.

With $\mathbf{S} = g(\alpha, \beta, \gamma)$, we write diagonal elements of $\mathbf{S}^T\mathbf{o}$ as

$$
\begin{aligned}
o_{11}(\alpha, \beta, \gamma) &= (\cos\alpha\cos\gamma - \sin\alpha\sin\gamma\cos\beta)o_{11} + (-\cos\alpha\sin\gamma - \sin\alpha\cos\gamma\cos\beta)o_{21} \\
&\quad +(\sin\alpha\sin\beta)o_{31}, \\
o_{22}(\alpha, \beta, \gamma) &= (\sin\alpha\cos\gamma + \cos\alpha\sin\gamma\cos\beta)o_{12} + (-\sin\alpha\sin\gamma + \cos\alpha\cos\gamma\cos\beta)o_{22} \\
&\quad +(-\cos\alpha\sin\beta)o_{32}, \text{ and} \\
o_{33}(\alpha, \beta, \gamma) &= (\sin\gamma\sin\beta)o_{13} + (\cos\gamma\sin\beta)o_{23} + (\cos\beta)o_{33}.
\end{aligned} \tag{9}
$$

where "o_{ij}" denotes components of $\mathbf{o}$.

3.2 Maximum quasi-likelihood estimation (MQL)

The singularity of (6) at $\mathbf{o} = \mathbf{S}$ means that the one-sample likelihood for the vM-UARS($\mathbf{S}$, κ) inference problem has singularities at $\mathbf{S}$ equal to each observation $\mathbf{o}_i$. So in place of inference based on the likelihood we consider quasi-likelihood-based inference based on quasi-density (7) for the one-sample problem for the vM-UARS($\mathbf{S}$, κ) distribution using the parameterization of $\mathbf{S}$ introduced in Section 3.1.

Suppose observations $\mathbf{o}_1, \ldots, \mathbf{o}_n \in \Omega$ are iid from the vM-UARS($\mathbf{S}$, κ) distribution. Then, we have quasi-likelihood function

$$L_n(\kappa, (\alpha, \beta, \gamma)) = [I_0(\kappa)]^{-n} \prod_{i=1}^{n} \exp\left[\frac{\kappa}{2}(o_{11,i}(\alpha, \beta, \gamma) + o_{22,i}(\alpha, \beta, \gamma) + o_{33,i}(\alpha, \beta, \gamma) - 1)\right] \tag{10}$$

where, as in (9), $o_{11,i}(\alpha, \beta, \gamma), o_{22,i}(\alpha, \beta, \gamma), o_{33,i}(\alpha, \beta, \gamma)$ denote the diagonal entries of $\mathbf{S}^T\mathbf{o}_i$, $i = 1, \ldots, n$, with $\mathbf{S} = g(\alpha, \beta, \gamma)$. The one-sample log-quasi-likelihood for the vM-UARS($\mathbf{S}$, κ) distribution is then

$$\begin{aligned} l_n(\kappa, (\alpha, \beta, \gamma)) &= \frac{\kappa}{2} \sum_{i=1}^{n} (o_{11,i}(\alpha, \beta, \gamma) + o_{22,i}(\alpha, \beta, \gamma) + o_{33,i}(\alpha, \beta, \gamma) - 1) - n \log(I_0(\kappa)) \\ &= \frac{\kappa n}{2} tr(\mathbf{S}^T \bar{\mathbf{o}}) - \frac{\kappa n}{2} - n \log(I_0(\kappa)), \end{aligned} \tag{11}$$

using the sample mean $\bar{\mathbf{o}} = \sum_{i=1}^{n} \mathbf{o}_i/n$. Thus, the maximum quasi-likelihood (MQL) estimates for (α, β, γ), say $(\hat{\alpha}, \hat{\beta}, \hat{\gamma})$, are such that $\hat{\mathbf{S}} = g(\hat{\alpha}, \hat{\beta}, \hat{\gamma})$ maximizes $tr(\mathbf{S}^T \bar{\mathbf{o}})$. Therefore, the MQL estimate $\hat{\mathbf{S}}$ for the vM-UARS($\mathbf{S}$, κ) distribution is the moment estimator mentioned in Section 1. Chang and Rivest (2001) also discuss M-Estimation for the location parameter $\mathbf{S}$ by minimizing objective functions that include those that are functions of $tr(\mathbf{S}^T\mathbf{o}_i)$, while Rivest and Chang (2006) consider regression-type estimators of the location parameter.

3.3 Asymptotic results

For later inference, we develop some asymptotic results for one-sample quasi-likelihood inference; all proofs appear in the supplementary on-line Appendix. Our first result regards the asymptotic distribution of the maximum quasi-likelihood (MQL) estimator.

Proposition 1. *Suppose* $\mathbf{O}_1, \ldots, \mathbf{O}_n$ *are iid vM-UARS(*$\mathbf{S}$*,* κ*). Let* $\hat{\boldsymbol{\theta}}_n^T$ *be the MQL estimator of* $\boldsymbol{\theta}^T = (\kappa, (\alpha, \beta, \gamma))$ *and suppose that the true value of* $\boldsymbol{\theta}$ *is* $\boldsymbol{\theta}_0$*. Then, under* $\boldsymbol{\theta}_0$

$$\sqrt{n}(\hat{\boldsymbol{\theta}}_n - \boldsymbol{\theta}_0) \xrightarrow{d} \text{MVN}(\mathbf{0}, H_1^{-1}(\boldsymbol{\theta}_0)\mathcal{I}_1(\boldsymbol{\theta}_0)H_1^{-1}(\boldsymbol{\theta_0})),$$

as $n \to \infty$*, where*

$$H_1(\boldsymbol{\theta}) \equiv \begin{pmatrix} \frac{I_2(\kappa)+\frac{1}{\kappa}I_1(\kappa)}{I_0(\kappa)} - \left(\frac{I_1(\kappa)}{I_0(\kappa)}\right)^2 & 0 & 0 & 0 \\ 0 & \kappa D(\kappa) & 0 & \kappa D(\kappa)\cos\beta \\ 0 & 0 & \kappa D(\kappa) & 0 \\ 0 & \kappa D(\kappa)\cos\beta & 0 & \kappa D(\kappa) \end{pmatrix} \tag{12}$$

and

$$\mathcal{I}_1(\boldsymbol{\theta}) \equiv \begin{pmatrix} \frac{I_2(\kappa)+\frac{1}{\kappa}I_1(\kappa)}{I_0(\kappa)} - \left(\frac{I_1(\kappa)}{I_0(\kappa)}\right)^2 & 0 & 0 & 0 \\ 0 & \frac{\kappa I_1(\kappa)}{3I_0(\kappa)} & 0 & \frac{\kappa I_1(\kappa)\cos\beta}{3I_0(\kappa)} \\ 0 & 0 & \frac{\kappa I_1(\kappa)}{3I_0(\kappa)} & 0 \\ 0 & \frac{\kappa I_1(\kappa)\cos\beta}{3I_0(\kappa)} & 0 & \frac{\kappa I_1(\kappa)}{3I_0(\kappa)} \end{pmatrix} \tag{13}$$

for $D(\kappa) = \frac{1}{3} + \frac{2}{3}\frac{I_1(\kappa)}{I_0(\kappa)}$ *and* $I_i(\kappa)$ *the modified Bessel function of order* i*.*

See the Appendix for expressions of $H_1(\boldsymbol{\theta})$ and $\mathcal{I}_1(\boldsymbol{\theta})$ in terms of expected derivatives for the log-quasi-likelihood.

We proceed to look at limiting distributions associated with two different methods of hypothesis testing. For Propositions 2 and 3 we derive the asymptotic null distributions of quasi-likelihood ratio test (Q-LRT) statistics and Wald type test statistics, while Propositions 4 and 5 concern non-null distributions for these statistics.

Proposition 2. *(Asymptotic Null Distributions of Quasi-Likelihood Ratio Test (Q-LRT) Statistics) Suppose that we partition* $\boldsymbol{\theta}_{4\times1}^T = (\kappa, (\alpha, \beta, \gamma))$ *into* $\begin{pmatrix} \boldsymbol{\theta}_1 \\ \boldsymbol{\theta}_2 \end{pmatrix}$ *where* $\boldsymbol{\theta}_1$ *is* $r \times 1$ *and* $\boldsymbol{\theta}_2$ *is* $(4-r)\times 1$*. Consider the hypothesis*

$$\mathrm{H}_0 : \boldsymbol{\theta}_1 = \boldsymbol{\theta}_{01}$$

where the true value of $\boldsymbol{\theta}$*,* $\boldsymbol{\theta}_0 = \begin{pmatrix} \boldsymbol{\theta}_{01} \\ \boldsymbol{\theta}_{02} \end{pmatrix}$*, satisfies* H_0*, and define* $\lambda_n = \dfrac{L_n(\boldsymbol{\theta}_n^*)}{L_n(\hat{\boldsymbol{\theta}}_n)}$*, where* L_n *is as in (10),* $\hat{\boldsymbol{\theta}}_n$ *is the MQL estimate over* Θ*, and* $\boldsymbol{\theta}_n^*$ *is the MQL estimate over* Θ_0 *(the part of the parameter space where* H_0 *holds). Then, as* $n \to \infty$*,*

$$-2\log(\lambda_n) \xrightarrow{d} \begin{cases} \chi_1^2 + B(\kappa_0)\chi_3^2 & \text{for} \quad \boldsymbol{\theta}_1 = \boldsymbol{\theta} \\ B(\kappa_0)\chi_3^2 & \text{for} \quad \boldsymbol{\theta}_1^T = (\alpha, \beta, \gamma) \\ \chi_1^2 & \text{for} \quad \boldsymbol{\theta}_1 = \kappa \end{cases} \tag{14}$$

where $B(\kappa_0) = \frac{I_1(\kappa_0)}{I_0(\kappa_0)+2I_1(\kappa_0)} \in \left(0, \frac{1}{3}\right]$ *and* χ_1^2 *and* χ_3^2 *are independent chi-squared variables.*

Proposition 3. *(Asymptotic Null Distribution of the Overall Wald Test Statistic) Consider the hypothesis* $\mathrm{H}_0 : \boldsymbol{\theta} = \boldsymbol{\theta}_0$*. Define*

$$T_n = n(\hat{\boldsymbol{\theta}}_n - \boldsymbol{\theta}_0)^T H_1(\boldsymbol{\theta}_0)\mathcal{I}_1^{-1}(\boldsymbol{\theta}_0)H_1(\boldsymbol{\theta}_0)(\hat{\boldsymbol{\theta}}_n - \boldsymbol{\theta}_0)$$

for $H_1(\boldsymbol{\theta})$ *and* $\mathcal{I}_1(\boldsymbol{\theta})$ *as in* (12) *and* (13)*, respectively. Then, under* H_0 *(under* Θ_0*), as* $n \to \infty$*,*

$$T_n \xrightarrow{d} \chi_4^2.$$

In a straightforward manner it also holds that if we wish to test $\mathrm{H}_0 : (\alpha, \beta, \gamma)^T = (\alpha_0, \beta_0, \gamma_0)^T$ and partition $H_1(\boldsymbol{\theta}_0)$ and $\mathcal{I}_1^{-1}(\boldsymbol{\theta}_0)$ accordingly, then under H_0 the Wald statistic $T_n \xrightarrow{d} \chi_3^2$ as $n \to \infty$. Similarly, for the test of $\mathrm{H}_0 : \kappa = \kappa_0$, under H_0 the Wald statistic $T_n \xrightarrow{d} \chi_1^2$.

Next, we will expand on the previous two propositions by finding limiting distributions of the overall Q-LRT statistic and overall Wald test statistic under local alternative hypotheses.

Proposition 4. *(Limiting Non-Null Distribution for the Overall Quasi-Likelihood Ratio Statistic) For* $\boldsymbol{\theta}^T = (\kappa, (\alpha, \beta, \gamma))$*, suppose* $\boldsymbol{\theta}_0$ *denotes the true parameter value and*

$$\tilde{\boldsymbol{\theta}}_n = \boldsymbol{\theta}_0 + H_1^{-1}(\boldsymbol{\theta}_0)\mathcal{I}_1(\boldsymbol{\theta}_0)^{\frac{1}{2}}\frac{\boldsymbol{\delta}}{\sqrt{n}} \tag{15}$$

for $\boldsymbol{\delta}^T = (\delta_k, \delta_\alpha, \delta_\beta, \delta_\gamma) \in \mathbb{R}^4$*. Let* $\lambda_n = \dfrac{L_n(\tilde{\boldsymbol{\theta}}_n)}{L_n(\hat{\boldsymbol{\theta}}_n)}$ *denote the quasi-likelihood ratio along the sequence* $\tilde{\boldsymbol{\theta}}_n$*, where* $\hat{\boldsymbol{\theta}}_n$ *is the MQL estimate of* $\boldsymbol{\theta}$*. Then under the sequence of nulls* $\tilde{\boldsymbol{\theta}}_n$*, as* $n \to \infty$*,*

$$-2\log(\lambda_n) \xrightarrow{d} \chi_1^2(\delta_\kappa^2) + B(\kappa_0)\chi_3^2(\delta_\alpha^2 + \delta_\beta^2 + \delta_\gamma^2),$$

for $B(\kappa_0) = \frac{I_1(\kappa_0)}{I_0(\kappa_0)+2I_1(\kappa_0)}$ *where* $\chi_1^2(\delta_\kappa^2)$ *and* $\chi_3^2(\delta_\alpha^2 + \delta_\beta^2 + \delta_\gamma^2)$ *are independent chi-squared random variables with noncentrality parameters* δ_κ^2 *and* $\delta_\alpha^2 + \delta_\beta^2 + \delta_\gamma^2$*.*

Note that if we rewrite Proposition 4 by replacing (15) with $\tilde{\boldsymbol{\theta}}_n = \boldsymbol{\theta}_0 + \dfrac{\boldsymbol{\delta}}{\sqrt{n}}$, we find that under the sequence of nulls $\tilde{\boldsymbol{\theta}}_n$,

$$-2\log(\lambda_n) \xrightarrow{d} \chi_1^2(\eta_1) + B(\kappa_0)\chi_3^2(\eta_2),$$

where $\chi_1^2(\eta_1)$ and $\chi_3^2(\eta_2)$ are independent chi-squared random variables with noncentrality parameters

$$\eta_1 = \delta_\kappa^2\left[\frac{I_2(\kappa_0) - \frac{1}{\kappa_0}I_1(\kappa_0)}{I_0(\kappa_0)} - \left(\frac{I_1(\kappa_0)}{I_0(\kappa_0)}\right)^2\right]$$

and

$$\eta_2 = \frac{I_1(\kappa_0)}{3\kappa_0 I_0(\kappa_0)}\left(1 + 2\frac{I_1(\kappa_0)}{I_0(\kappa_0)}\right)^2\left[\delta_\alpha^2 + \delta_\beta^2 + \delta_\gamma^2 + 2\delta_\alpha\delta_\gamma\cos\beta_0\right].$$

With $\tilde{\mathbf{S}}_n = g(\tilde{\alpha}_n, \tilde{\beta}_n, \tilde{\gamma}_n)$ and $\mathbf{S}_0 = g(\alpha_0, \beta_0, \gamma_0)$, where g is as in (8), suppose ξ_n is the misorientation angle between $\tilde{\mathbf{S}}_n$ and $\mathbf{S}_0$. Then, $n(2 - 2\cos\xi_n) \xrightarrow{p} \delta_\alpha^2 + \delta_\beta^2 + \delta_\gamma^2 + 2\delta_\alpha\delta_\gamma\cos\beta_0$, so the part of the noncentrality parameter η_2 not depending on κ_0 is obtained as the limit of a function of this misorientation angle.

Proposition 5. *(Limiting Non-Null Distribution for the Overall Wald Test Statistic) For* $\boldsymbol{\theta}^T = (\kappa, (\alpha, \beta, \gamma))$*, suppose* $\boldsymbol{\theta}_0$ *denotes the true parameter value and*

$$\tilde{\boldsymbol{\theta}}_n = \boldsymbol{\theta}_0 + H_1^{-1}(\boldsymbol{\theta}_0)\mathcal{I}_1(\boldsymbol{\theta}_0)^{\frac{1}{2}}\frac{\boldsymbol{\delta}}{\sqrt{n}}$$

for $\boldsymbol{\delta}^T = (\delta_k, \delta_\alpha, \delta_\beta, \delta_\gamma) \in \mathbb{R}^4$. *Then under the sequence of nulls* $\tilde{\boldsymbol{\theta}}_n$, *as* $n \to \infty$,

$$T_n \xrightarrow{d} \chi^2_4(\delta_\kappa^2 + \delta_\alpha^2 + \delta_\beta^2 + \delta_\gamma^2).$$

3.4 Confidence regions

We can obtain confidence regions for $\mathbf{S}$ or κ by inversion of either quasi-likelihood ratio or Wald tests. This results in confidence intervals for κ. For $\mathbf{S}$, inversion of tests of $\mathrm{H}_0 : (\alpha, \beta, \gamma) = (\alpha_0, \beta_0, \gamma_0)$ produces the set of triples $(\alpha_0, \beta_0, \gamma_0)$ for which the test statistic is small. Applying the function g from (8) to all such triples gives a set of orientations comprising the confidence set for $\mathbf{S}$. Letting $\hat{\mathbf{S}}$ denote the MQL estimate of $\mathbf{S}$, the angle between each of the 3 perpendicular axes representing an orientation in the confidence set and the corresponding axis of $\hat{\mathbf{S}}$ can be found. Let ρ be the maximum of all such angles (found numerically). We consider a confidence region for $\mathbf{S}$ (potentially slightly more conservative than that resulting from inversion of the tests) as the set of all orientations for which the maximum angle between an $\mathbf{S}$ coordinate axis and an $\hat{\mathbf{S}}$ coordinate axis is less than ρ. We can represent this confidence region by 3 cones of constant angle ρ around axes representing $\hat{\mathbf{S}}$ and the notion of "size" of the confidence region for $\mathbf{S}$ can be reduced to thinking about the size of ρ. In Section 4 we give confidence intervals for κ and figures representing confidence regions for $\mathbf{S}$ based on data from the vM-UARS($\mathbf{S}$, κ) distribution.

4 Simulation study and asymptotic power comparison

To investigate the relevance of the asymptotic results of Section 3.3 to statistical practice, we simulated data from the vM-UARS($\mathbf{S}$, κ) distribution using different choices for the parameter κ for various sample sizes. The values used for κ were 2, 8, and 20 and sample sizes were $n = 10, 30, 100$, and 300. The values used for α, β, and γ in $\mathbf{S} = g(\alpha, \beta, \gamma)$, where g is as in (8), were fixed at respectively 2.3, 1.1, and 5.9 throughout the simulations (though simple symmetry arguments show that this detail is immaterial).

We simulated 1000 samples for each (n, κ) combination and obtained values for the Q-LRT statistic and the Wald test statistic, for testing for the entire parameter vector. The empirical cumulative distribution function for each test statistic was then plotted along with the limiting distribution. Figure 6 contains the plots for $\kappa = 2$ and 8 (similar plots resulted for $\kappa = 20$).

The asymptotic cutoff for the Q-LRT for the entire vector with $\kappa = 8$, and at an α-level of 0.05, is (based on Proposition 2) approximately 5.123. From the empirical cumulative distribution functions represented in Figure 6 we find that this value corresponds to α-levels of approximately 0.0565, 0.055, 0.053, and 0.052 for $n = 10, 30, 100$, and 300, respectively. So, when using the asymptotic cutoff with small sample sizes, the actual levels are more liberal than the desired $\alpha = 0.05$. The asymptotic cutoff for the Wald test for the entire vector, at an α-level of 0.05, is (based on Proposition 3) approximately 9.488. From the empirical cumulative distribution functions, we find that this value corresponds to α-levels of approximately 0.173, 0.093, 0.072, and 0.057 for $n = 10, 30, 100$ and 300, respectively, when $\kappa = 8$. Thus, the convergence in the case of the Wald test is not as fast as for the Q-LRT. Similar results hold for $\kappa = 2$ and 20, and when testing for only κ. When testing for only the set (α, β, γ) the results for both the Wald test and the Q-LRT are similar to those of the Q-LRT of the entire parameter vector.

It is also instructive to consider MQL estimates for one sample of size $n = 30$ simulated from the vM-UARS($\mathbf{S}$, κ) distribution under each of the 3 values of κ (where again where $\mathbf{S} = g(2.3, 1.1, 5.9)$). MQL estimates obtained from each of these three samples are presented in Table 3.

Table 3: Maximum quasi-likelihood estimates for samples of size 30

	$\hat{\kappa}$	$\hat{\alpha}$	$\hat{\beta}$	$\hat{\gamma}$
$\kappa = 2$	2.524342	2.275942	1.052625	5.931470
$\kappa = 8$	8.066815	2.290575	1.077529	5.876191
$\kappa = 20$	18.297676	2.305525	1.136357	5.892312

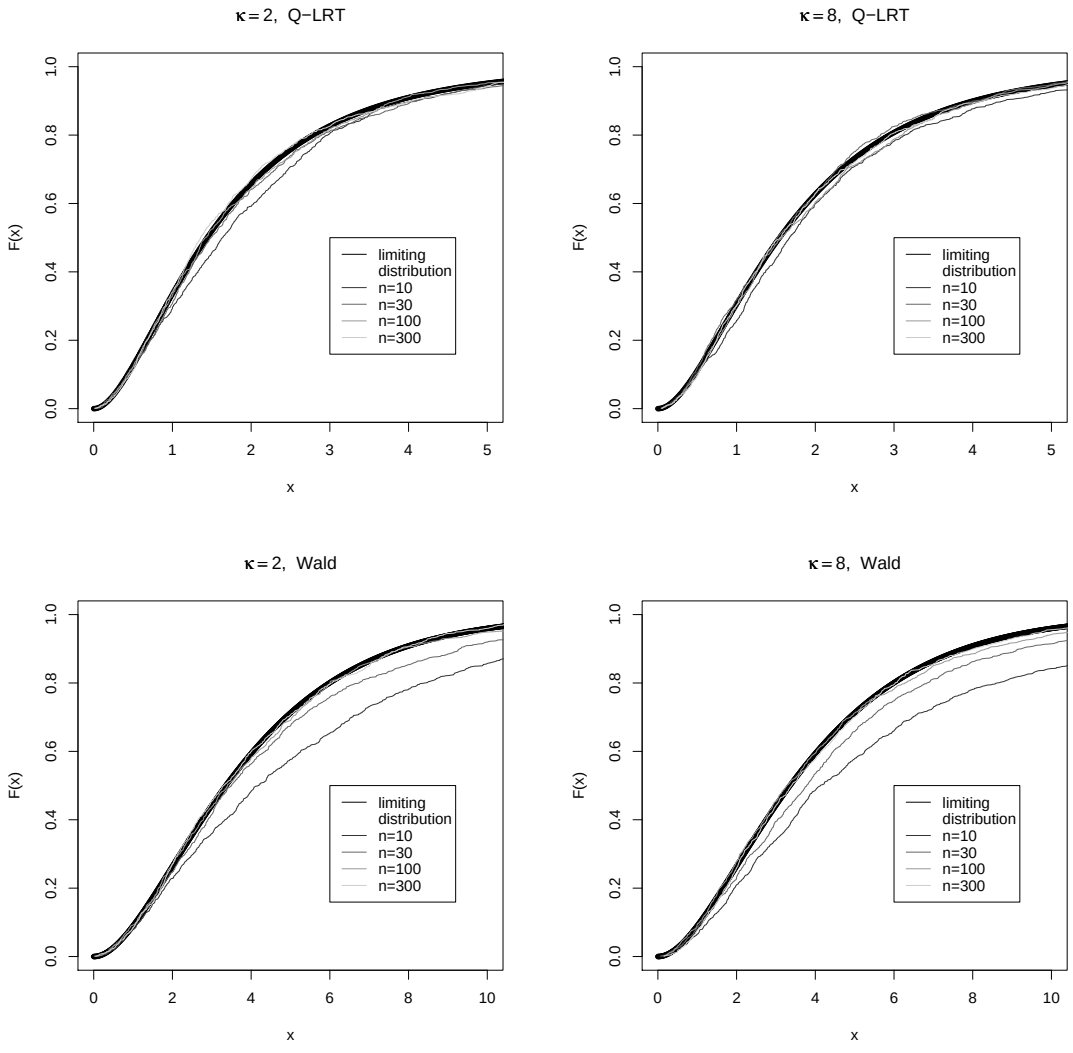

Figure 6: Limiting and empirical (estimated small n) null cumulative distribution functions for the Q-LRT (top) and Wald (bottom) statistics for the full parameter vector, $\kappa = 2$ (right) and 8 (left)

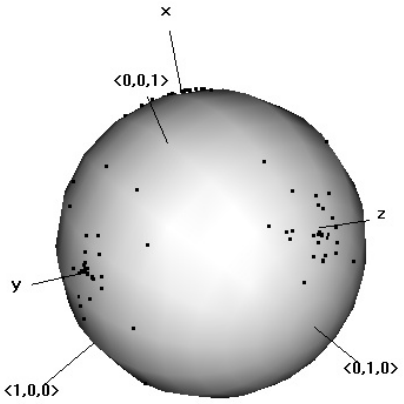

Figure 7: Spherical representation of $n = 30$ vM-UARS($\mathbf{S}$, 8) data points (x, y, and z represent the axes of the MQL estimate of $\mathbf{S}$)

To graphically portray such data and the corresponding MQL estimate of $\mathbf{S}$, we display the data on a 3-dimensional sphere. Figure 7 shows the 30 realizations from the vM-UARS($\mathbf{S}$, 8) distribution as points on a sphere corresponding to the positions of the x, y, and z unit vectors after rotation. The orientation given by the MQL estimate of $\mathbf{S}$ is portrayed by the axes at x, y, and z. We see from Figure 7 that the MQL estimate of $\mathbf{S}$ is "in the center" of the data.

We can also give confidence regions based on inversion of both quasi-likelihood ratio and Wald tests. 95% confidence limits for the parameter κ under each of these methods are presented in Table 4. We represent the 95% quasi-likelihood ratio confidence region for $\mathbf{S}$ in Figure 8 using the method described in Section 3.4. Here, the axes at x, y, and z represent the orientation of the MQL estimate for $\mathbf{S}$, as given by $\hat{\mathbf{S}} = g(\hat{\alpha}, \hat{\beta}, \hat{\gamma})$. We note that in the limiting distribution given in (14), the quantity $B(\kappa_0) = \frac{I_1(\kappa_0)}{I_0(\kappa_0)+2I_1(\kappa_0)}$ is bounded above by $\frac{1}{3}$. So, when making the 95% quasi-likelihood ratio confidence region for (α, β, γ) we used the upper 5% point of the "$\frac{1}{3}\chi^2_3$" distribution as the cutoff between small and large values of $-2\log(\lambda_{30})$. By comparing the plots in Figure 8, we see that for larger values of κ, since the data are more concentrated, we get smaller conic regions. The angle between each axis and the edge of the conic region is 0.19278 for $\kappa = 2$, 0.09862 for $\kappa = 8$, and 0.07174 for $\kappa = 20$. Although we do not present a corresponding figure here, in the case of a 95% Wald

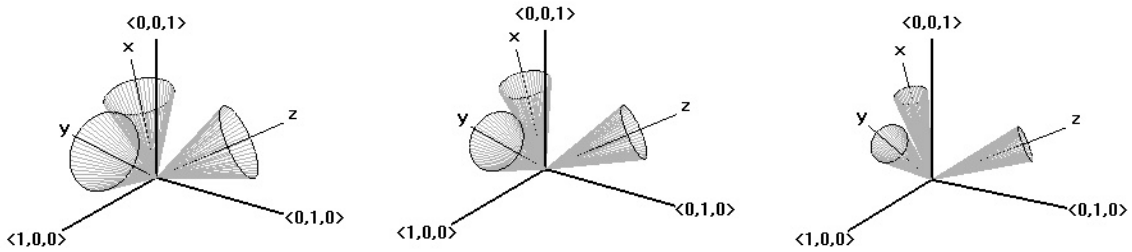

Figure 8: 95% Quasi-likelihood ratio confidence regions for $\mathbf{S}$ based on samples of $n = 30$ ($\kappa = 2, 8$, and 20, left to right)

confidence region, these angles are 0.18199, 0.09709, and 0.07025, respectively.

Table 4: 95% Confidence limits for the parameter κ

	Quasi-likelihood ratio	Wald
$\kappa = 2$	(1.571072, 3.796212)	(1.733614, 4.735426)
$\kappa = 8$	(4.777156, 12.69225)	(5.470979, 16.05493)
$\kappa = 20$	(10.64507, 29.02341)	(12.24265, 36.77996)

Using Propositions 4 and 5 we can compare the asymptotic power of the quasi-likelihood ratio and Wald theory tests (for the entire parameter vector) under various choices of κ_0 and $\boldsymbol{\delta}$. Table 5 gives the limiting power of each test (at a limiting α-level of 0.05) for some combinations of these values. In checking various combinations of κ_0 and $\boldsymbol{\delta}$, the Q-LRT generally tended to have more asymptotic power than the Wald test in cases where the largest deviation between true and null-hypothesized parameters was located in the spread parameter κ_0; when the greatest deviations were located in the Euler angle parameters, the Wald test had better large sample power. Each test has its own strengths. The explanation is that the limit law of the quasi-likelihood ratio statistic is a convolution of two chi-squared variables where deviations between hypothesized and true parameters are split into different noncentrality parameters, depending on the location of the deviations (i.e., whether these lie in the concentration parameter κ or in the location/Euler angle parameters). In contrast, the chi-squared limit in the Wald test has one noncentrality parameter that combines all

deviations between true and hypothesized parameters.

Table 5: Asymptotic power of the quasi-likelihood ratio and Wald tests (for the entire vector) under various choices of κ_0 and $\boldsymbol{\delta}$

$\boldsymbol{\delta}$	Q-LRT			Wald
	$\kappa_0 = 1$	$\kappa_0 = 4$	$\kappa_0 = 16$	
$(.1, .1, .1, .1)$	0.0504	0.0507	0.0510	0.0520
$(1, .1, .1, .1)$	0.1665	0.1619	0.1617	0.1073
$(2, .1, .1, .1)$	0.5041	0.4834	0.4786	0.3224
$(.1, 1, 1, 1)$	0.0984	0.1218	0.1277	0.2449
$(.1, 2, 2, 2)$	0.4109	0.5500	0.5623	0.8028
$(1, 1, 1, 1)$	0.2278	0.2603	0.2622	0.3201
$(2, 1, 1, 1)$	0.5814	0.5912	0.5934	0.5400
$(2, 2, 2, 2)$	0.7997	0.8506	0.8530	0.9119

5 Application of quasi-likelihood methodology for the von Mises version of the UARS distributions to the crystal orientation data

As promised in Section 1, we examine the repeatability of measurements obtained using EBSD. As our matrix models describe rotational symmetry, we calculated the value of Prentice's R statistic for each data set. Small values were found, suggesting that an assumption of spherical symmetry is reasonable in all cases (see Prentice, 1984). We then fit the von Mises version of the Uniform-Axis-Random-Spin distributions to the 14 repeat nickel observations in Table 1 and seven repeat aluminum observations via MQL. Because the data were so highly concentrated around their principal directions, the MQL estimates of the parameters κ were extremely large. Thus, we used the normal approximation to the von Mises distribution as given in Section 2.2 for computing the quasi-likelihood. Estimates and 95% confidence intervals for κ are provided in Table 6. The estimates for the location $\mathbf{S}$ (represented as Euler angles $(\alpha,\ \beta,\ \gamma)$) are $(5.8620,\ 0.9352,\ 4.2170)$ and $(5.3552,\ 1.4566,\ 0.0580)$ for the nickel and aluminum data, respectively. (We will not present a figure giving the confidence region for $\mathbf{S}$ as we did in the previous section. The region is so small that it visually appears as a "corner" positioned at the estimated principal direction instead of as

a set of a conic regions).

Table 6: MQL estimates and 95% confidence limits for the parameter κ for the repeat nickel and aluminum data sets

	MQL estimate	Q-LRT interval	Wald interval
Nickel	86373.7613	(37113.27, 167042.84)	(49617.48, 333217.06)
Aluminum	58829.1138	(994.2512, 70864.1789)	(28730.26, 14120080)

The intervals for κ given in Table 6 contain only values that represent highly concentrated distributions on Ω. To put the estimated values of κ into the context of EBSD precision, we consider the normal approximation to the von Mises circular distribution. Under this approximation, with $\hat{\kappa}$ the MQL estimate for a set of data, the spin angles r effectively follow a normal distribution with mean 0 and variance $1/\hat{\kappa}$. Thus, the angles r for the repeated nickel data are approximately normal with standard deviation 0.003402 radians, or 0.19495°. So, the corresponding fitted distribution on the misorientation angles $|r|$ places 99% probability in the interval (0°, 0.5022°), giving an EBSD precision of 0.5022°. For the repeated aluminum data, the angles r are approximately normal with standard devation 0.004123 radians, or 0.23623°, and the fitted distribution on the misorientation angles places 99% probability in the interval (0°, 0.6085°) for an EBSD precision of 0.6085°. Therefore, both metals produce single-site estimated EBSD precisions better than the literature-standard 1°. But again note that EBSD precisions given in the literature are based on a single scan across a homogeneous specimen and not repeat readings at a given location. Our present analysis provides more optimistic precisions than those in the literature when pure repeatability is at issue.

Next, we consider measurements from a single scan that appear to be within the same grain. With 70 different locations for the nickel data we arrive at a MQL estimate for $\mathbf{S}$ given by the Euler angles (5.8544, 0.9297, 4.2224). With 50 different locations for the aluminum data, we arrive at an estimate of (5.3521, 1.4506, 0.0585). We expect the observations to be highly concentrated about the principal directions. Estimates and 95% confidence intervals

for κ are provided in Table 7.

Table 7: MQL estimates and 95% confidence limits for the parameter κ for the within-grain nickel and aluminum data sets

	MQL estimate	Q-LRT interval	Wald interval
Nickel	19018.6767	(13393.45, 26033.30)	(14285.92, 28440.91)
Aluminum	30713.9345	(20193.15, 44375.14)	(22064.79, 50515.57)

Based on the estimated values of κ, the angles r for the nickel data are approximately normal with standard deviation 0.007251 radians, or 0.41546°, and the angles r for the aluminum data are approximately normal with standard deviation 0.005706 radians, or 0.32693°. Fitted distributions on the misorientation angles $|r|$ place 99% probability in the intervals (0°, 1.0701°) and (0°, 0.8421°), respectively. Thus, for the metals considered here, we obtain precision figures comparable to the commonly quoted 1° when considering observations representing different locations in a single grain. We emphasize, however, that our methods provide a coherent fitting and inference framework for this problem, where existing published work on EBSD precision is entirely descriptive and to some degree ad hoc in terms of how sets of measurements are converted to precision statements. The fact that pure repeatability variation (single site precision) for EBSD is smaller than between location variation even in a single crystal/grain is probably traceable to small effects of both 1) slight inhomogeneity of actual material properties site to site (for example, due to preparation differences across a specimen) and 2) slight inhomogeneity of equipment behavior site to site (related, for example, to physical distortions, discreteness of pixel locations on the focal plane, slightly different geometries of beam paths, etc.).

6 Conclusion

The UARS class of distributions and the inference tools developed in this paper are extremely attractive and provide alternatives for modeling 3-dimensional rotations beyond the distributions previously studied in the literature. This has proved valuable in our applica-

tion, allowing us to rationally and systematically quantify precision of EBSD measurements. The UARS models are tractable and have directly interpretable ("location" and "spread") parameters ($\mathbf{S}$ and κ). The motivating construction shows how to easily simulate from a UARS distribution, a fact that is proving to be extremely valuable in Bayes MCMC analyses (see Bingham, Vardeman, and Nordman, 2009 and Bingham, Nordman, and Vardeman, 2009). Our development of quasi-likelihood theory for the von Mises case is important in its own right and can serve as a template for parallel developments with other circular distributions (including those that lead to bounded densities, allowing for explicit likelihood theory) to provide a rich variety of alternative practical one-sample models for random orientations (see Bingham, Nordman, and Vardeman (2009) for likelihood and Bayes results for the symmetric matrix Fisher model based on the methods of the present paper). We can provide useful "one-way random effects" methods (see again Bingham, Vardeman, and Nordman (2009) and Bingham, Nordman, and Vardeman (2009)) and fully expect to provide simple "time series" and clustering methods for 3-dimensional rotations based on this class of distributions.

While much good and difficult work as been done on the problem of modeling randomness of rotations (Downs 1972; Khatri and Mardia 1977; Jupp and Mardia 1979; Prentice 1986; Mardia and Jupp 1999; Rancourt et al. 2000; Chang and Rivest 2001; Chikuse 2003; León et al. 2006; Rivest et al. 2008) our contention here is that focus on the UARS class provides heretofore unavailable flexibility and tractability that can open myriad possibilities in the analysis of 3-dimensional orientation data arising from various applications.

Acknowledgment

The authors wish to thank Dr. Barbara Lograsso of Michigan Technological University for introducing us to the EBSD problem and Fran Laabs of Ames Laboratory, Iowa State University, for collecting the EBSD data. We further thank Iowa State University Professor Max Morris for an early suggestion that led us to identify and study the UARS class.

Appendix: Properties of the UARS Distributions

We establish some properties of UARS distributions; proofs of these can be found in a supplementary on-line Appendix. For simplicity, some properties are stated only for the case of principle direction $\mathbf{I}_{3\times3}$. These may be easily extended to general $\mathbf{S}$ using the fact that $\mathbf{O} \sim \text{UARS}(\mathbf{I}_{3\times3}, \kappa)$ implies $\mathbf{S}\cdot\mathbf{O} \sim \text{UARS}(\mathbf{S}, \kappa)$. Further, note that while Properties 7 - 11 below are those of the von Mises version of the UARS distributions, Properties 1 - 6 hold for *any* choice of circular distribution $r \sim \text{Circ}(\kappa)$ (symmetric about 0 or not). Additionally, the last three properties concern the score function from the quasi-density and are relevant to the inference method described in Section 3.

Property 1. *If* $\mathbf{O} \sim$ *UARS*$(\mathbf{I}_{3\times3}, \kappa)$*, then* $\mathbf{O}^T \sim$ *UARS*$(\mathbf{I}_{3\times3}, \kappa)$*.*

Property 2. *If* $\mathbf{O} \sim$ *UARS*$(\mathbf{I}_{3\times3}, \kappa)$*, then* $\mathbf{S}\cdot\mathbf{O}\cdot\mathbf{S}^T \sim$ *UARS*$(\mathbf{I}_{3\times3}, \kappa)$ *for any* 3×3 *rotation matrix* $\mathbf{S}$*.*

Property 3. *If* $\mathbf{O} \sim$ *UARS*$(\mathbf{I}_{3\times3}, \kappa)$*, then* $\mathbf{S}\cdot\mathbf{O}$ *and* $\mathbf{O}\cdot\mathbf{S} \sim$ *UARS*$(\mathbf{S}, \kappa)$*.*

Property 4. *If* $\mathbf{O} \sim$ *UARS*$(\mathbf{S}, \kappa)$*, then* $\mathbf{O}^T \sim$ *UARS*$(\mathbf{S}^T, \kappa)$*.*

Property 5. *If* $\mathbf{O} \sim$ *UARS*$(\mathbf{S}, \kappa)$*, then* $\mathbf{S}^T\cdot\mathbf{O}$ *and* $\mathbf{O}\cdot\mathbf{S}^T \sim$ *UARS*$(\mathbf{I}_{3\times3}, \kappa)$*.*

Property 6. *Suppose* $\mathbf{O} \sim$ *UARS*$(\mathbf{I}_{3\times3}, \kappa)$ *and* $\mathbf{O} = (\mathbf{X}\ \mathbf{Y}\ \mathbf{Z})$*, where* $\mathbf{X}, \mathbf{Y}$*, and* $\mathbf{Z}$ *are the three columns of* $\mathbf{O}$*. Let* P_X *be the spherical distribution of* $\mathbf{X}$ *about* $(1,0,0)^T$*,* P_Y *be the spherical distribution of* $\mathbf{Y}$ *about* $(0,1,0)^T$*, and* P_Z *be the spherical distribution of* $\mathbf{Z}$ *about* $(0,0,1)^T$*. Then* $P_X = P_Y = P_Z$*.*

Property 7. *If* $\mathbf{O} \sim$ *vM-UARS*$(\mathbf{I}_{3\times3}, \kappa)$*, then*

$$\text{E}(\mathbf{O}) = \left(\frac{1}{3} + \frac{2}{3}\frac{I_1(\kappa)}{I_0(\kappa)}\right)\mathbf{I}_{3\times3}, \qquad \text{E}(\mathbf{O^2}) = \left(\frac{1}{3} + \frac{2}{3}\frac{I_2(\kappa)}{I_0(\kappa)}\right)\mathbf{I}_{3\times3},$$

where $I_i(\kappa)$ *is the modified Bessel function of order* i*.*

Property 8. *Suppose* $\mathbf{O} = (\mathbf{X}\ \mathbf{Y}\ \mathbf{Z}) \sim$ *vM-UARS*$(\mathbf{I}_{3\times 3}, \kappa)$. *Let* x *represent the cosine of the angle between* $\mathbf{X}$ *and* $(1,0,0)^T$, y *represent the cosine of the angle between* $\mathbf{Y}$ *and* $(0,1,0)^T$, *and* z *represent the cosine of the angle between* $\mathbf{Z}$ *and* $(0,0,1)^T$. *Then,*

$$\mathrm{Corr}(x,y) = \mathrm{Corr}(x,z) = \mathrm{Corr}(y,z) = \frac{\frac{1}{15} + \frac{8}{15}\frac{I_1(\kappa)}{I_0(\kappa)} + \frac{2}{5}\frac{I_2(\kappa)+\frac{1}{\kappa}I_1(\kappa)}{I_0(\kappa)} - \left(\frac{1}{3} + \frac{2}{3}\frac{I_1(\kappa)}{I_0(\kappa)}\right)^2}{\frac{1}{5} + \frac{4}{15}\frac{I_1(\kappa)}{I_0(\kappa)} + \frac{8}{15}\frac{I_2(\kappa)+\frac{1}{\kappa}I_1(\kappa)}{I_0(\kappa)} - \left(\frac{1}{3} + \frac{2}{3}\frac{I_1(\kappa)}{I_0(\kappa)}\right)^2}.$$

Property 9. *Suppose that* $\mathbf{O} \sim$ *vM-UARS*$(\mathbf{S}, \kappa)$. *If* $l(\kappa,(\alpha,\beta,\gamma)) = l_1(\kappa,(\alpha,\beta,\gamma))$ *as in* (11) *and*

$$l'(\kappa,(\alpha,\beta,\gamma)) = \left(\frac{\partial l}{\partial \kappa}, \ \frac{\partial l}{\partial \alpha}, \ \frac{\partial l}{\partial \beta}, \ \frac{\partial l}{\partial \gamma} \right)^T,$$

then $\mathrm{E}(l'(\kappa,(\alpha,\beta,\gamma))) = \mathbf{0}$.

Property 10. *Suppose that* $\mathbf{O} \sim$ *vM-UARS*$(\mathbf{S}, \kappa)$ *and that*

$$l''(\kappa,(\alpha,\beta,\gamma)) = \begin{pmatrix} \frac{\partial^2 l}{\partial \kappa^2} & \frac{\partial^2 l}{\partial \kappa \partial \alpha} & \frac{\partial^2 l}{\partial \kappa \partial \beta} & \frac{\partial^2 l}{\partial \kappa \partial \gamma} \\ \frac{\partial^2 l}{\partial \kappa \partial \alpha} & \frac{\partial^2 l}{\partial^2 \alpha} & \frac{\partial^2 l}{\partial \alpha \partial \beta} & \frac{\partial^2 l}{\partial \alpha \partial \gamma} \\ \frac{\partial^2 l}{\partial \kappa \partial \beta} & \frac{\partial^2 l}{\partial \alpha \partial \beta} & \frac{\partial^2 l}{\partial^2 \beta} & \frac{\partial^2 l}{\partial \alpha \partial \gamma} \\ \frac{\partial^2 l}{\partial \kappa \partial \gamma} & \frac{\partial^2 l}{\partial \alpha \partial \gamma} & \frac{\partial^2 l}{\partial \beta \partial \gamma} & \frac{\partial^2 l}{\partial^2 \gamma} \end{pmatrix}$$

for $l(\kappa,(\alpha,\beta,\gamma))$ *as in Property 9. Then,* $H_1(\kappa,(\alpha,\beta,\gamma)) = -\mathrm{E}(l''(\kappa,(\alpha,\beta,\gamma))$ *is as given in* (12).

Property 11. *Suppose that* $\mathbf{O} \sim$ *vM-UARS*$(\mathbf{S}, \kappa)$ *and that*

$$l'(\kappa,(\alpha,\beta,\gamma)) = \left(\frac{\partial l}{\partial \kappa}, \ \frac{\partial l}{\partial \alpha}, \ \frac{\partial l}{\partial \beta}, \ \frac{\partial l}{\partial \gamma} \right)^T$$

for $l(\kappa,(\alpha,\beta,\gamma))$ *as in Property 9. Then,* $\mathcal{I}_1(\kappa,(\alpha,\beta,\gamma)) = \mathrm{Var}(l'(\kappa,(\alpha,\beta,\gamma))$ *is as given in* (13).

References

Bingham, M. A., Nordman, D. J., and Vardeman, S. B. (2009) "Likelihood and Bayes Inference for the Symmetric von Mises-Fisher Distribution," Preprint, Department of Statistics, Iowa State University.

Bingham, M. A., Vardeman, S. B., and Nordman, D. J. (2009) "Bayes One-Sample and One-Way Random Effects Analyses for 3-D Orientations with Application to Materials Science," Preprint, Department of Statistics, Iowa State University.

Chang, T. and Rivest, L.-P. (2001), "M-Estimation for Location and Regression Parameters in Group Models: A Case Study Using Stiefel Manifolds," *The Annals of Statistics*, 29, 784-814.

Chikuse, Y. (2003), *Statistics on Special Manifolds*, New York: Springer.

Demirel, M. C., El-Dasher, B. S., Adams, B. L., and Rollett, A. D. (2000), "Studies on the Accuracy of Electron Backscatter Diffraction Measurements," in *Electron Backscatter Diffraction in Materials Science*, eds. Schwartz, A. J., Mukul, K., and Adams, B. L., New York: Kluwer Academic/Plenum Publishers.

Downs, T. D. (1972), "Orientation Statistics," *Biometrika*, 59, 665-676.

Jupp, P. E., and Mardia, K. V. (1979), "Maximum Likelihood Estimators for the Matrix Von Mises-Fisher and Bingham Distributions," *The Annals of Statistics*, 7, 599-606.

Khatri, C. G., and Mardia, K. V. (1977), "The Von Mises-Fisher Matrix Distribution in Orientation Statistics," *Journal of the Royal Statistical Society*, Ser. B, 39, 95-106.

León, C. A., Massé, J.-C., and Rivest, L.-P. (2006), "A Statistical Model for Random Rotations," *Journal of Multivariate Analysis*, 97, 412-430.

Mardia, K. V., and Jupp, P. E. (2000), *Directional Statistics*, Chichester; New York: John Wiley & Sons.

Miles, R. E. (1965), "On Random Rotations in R^3," *Biometrika*, 52, 636-639.

Morawiec, A. (2004), *Orientations and Rotations: Computations in Crystallographic Textures*, Berlin; New York: Springer.

Prentice, M. J. (1984), "A Distribution-Free Method of Interval Estimation for Unsigned Directional Data," *Biometrika*, 71, 147-154.

Prentice, M. J. (1986), "Orientation Statistics without Parametric Assumptions," *Journal of the Royal Statistical Society*, Ser. B, 48, 214-222.

Rancourt, D., Rivest, L.-P., Asselin, J. (2000), "Using Orientation Statistics to Investigate Variations in Human Kinematics," *Journal of the Royal Statistical Society*, Ser. C, 49, 81-94.

Randle, V. (2003), *Microtexture Determination and its Applications*, London: Maney for The Institute of Materials, Minerals and Mining.

Rivest, L.-P., Baillargeon, S., and Pierrynowski, M. (2008) "A Directional Model for the Estimation of the Rotation Axes of the Ankle Joint," *Journal of the American Statistical Association*, 103, 1060-1069.

Rivest, L.-P. and Chang, T. (2006), "Regression and Correlation for 3×3 Rotation Matrices," *The Canadian Journal of Statistics*, 34, 187-202.

Watson, G. S. (1983), *Statistics on Spheres*, New York: John Wiley & Sons.

Wilson, A. W. and Spanos, G. (2001), "Application of Orientation Imaging Microscopy to Study Phase Transformations in Steels," *Materials Characterization*, 46, 407-418.

Supplementary Material: MODELING AND INFERENCE FOR MEASURED CRYSTAL ORIENTATIONS AND A TRACTABLE CLASS OF SYMMETRIC DISTRIBUTIONS FOR ROTATIONS IN 3 DIMENSIONS

Supplementary material to follow consists of on-line Appendices A – D providing the development of the UARS density, proofs of the main results in the Appendix and Section 3.3 of the main manuscript, and Q-Q plots of EBSD aluminum data similar to those presented for the nickel data in Section 1 of the main manuscript.

On-line Appendix A: Development of the UARS density

Suppose that $\mathbf{O} \sim \text{UARS}(\mathbf{S}, \kappa)$ as in (3). Note that we may obtain an observation from UARS($\mathbf{S}$, κ) equivalently as

$$\mathbf{O} = \mathbf{S} \cdot M(\mathbf{U}, |r|). \tag{A.1}$$

The distributional equivalence of $\mathbf{S} \cdot M(\mathbf{U}, r)$ and $\mathbf{S} \cdot M(\mathbf{U}, |r|)$ follows from the fact that $M(\mathbf{U}, r) = M(-\mathbf{U}, -r)$ in (2) and that $\mathbf{U}$ is uniformly distributed and independent of r (see also Miles, 1965). Hence, we may develop a UARS($\mathbf{S}$, κ) density by considering the joint distribution of $(|r|, \mathbf{U})$. In this framework, every potential realization of $\mathbf{O}$ as in (A.1), for which $\mathbf{O} \neq \mathbf{S}$, corresponds to a unique realization of $\mathbf{U}$ and $|r| > 0$. In the case $\mathbf{O} = \mathbf{S}$, $r = 0$ and $M(\mathbf{U}, |r|) = \mathbf{I}_{3\times 3}$ hold.

To derive a density for a UARS($\mathbf{S}$, κ) distribution with respect to the invariant Haar measure, H, which acts as a "uniform distribution" on Ω (see Miles, 1965; Downs, 1972), first note that the uniform distribution for $\mathbf{U}$ on the unit sphere can be specified by allowing ϕ and $\tau \equiv \cos\theta$ in (1) to be independently and uniformly distributed on $[0, 2\pi]$ and $[-1, 1]$, respectively. If $r \in (-\pi, \pi]$ is also independently distributed with a density $C(r|\kappa)$ symmetric about 0, then $|r|$ has density $2 \cdot C(|r||\kappa)$, $|r| \in [0, \pi]$. Thus, a distribution F^* on $[-1, 1] \times [0, 2\pi] \times [0, \pi]$ for $(\tau, \phi, |r|)$ has a joint density $dF^*/d\lambda = C(|r||\kappa)/(2\pi)$, where λ stands for

3-dimensional Lebesgue measure. By definition, this distribution induces a corresponding distribution, F, for $\mathbf{O} = M(\mathbf{U}, |r|)$ in Ω that is UARS($\mathbf{I}_{3\times 3}$, κ). Recall that the mapping $\mathbf{O} = M(\mathbf{U}, |r|)$ is one-to-one (except for $r = 0$, an event of probability 0) so that $M^{-1}(\mathbf{O}) = (\mathbf{U}, |r|) \equiv (\tau, \phi, |r|)$ is essentially well-defined and the trace of $\mathbf{O}$ yields

$$|r| = \arccos\left[2^{-1}(tr(\mathbf{O}) - 1)\right]. \tag{A.2}$$

In the particular case where $|r|$ has a Lebesgue density $(1-\cos|r|)/\pi$, we obtain a distribution H^* on $[-1, 1] \times [0, 2\pi] \times [0, \pi]$ for $(\tau, \phi, |r|)$, which induces the Haar measure H on Ω via (A.1); see Miles (1965). Therefore, substituting (A.2) into

$$\frac{dF^*}{dH^*} = \frac{dF^*}{d\lambda}\frac{d\lambda}{dH^*} = \frac{2\pi C(|r||\kappa)}{1-\cos|r|}, \quad \tau \in [-1, 1],\ \phi \in [0, 2\pi],\ |r| \in [0, \pi] \tag{A.3}$$

gives the density $f = dF/dH$ of the UARS($\mathbf{I}_{3\times 3}$, κ) distribution on Ω with respect to H as

$$f(\mathbf{o}|\kappa) = \frac{4\pi}{3 - tr(\mathbf{o})} C\left(\arccos[2^{-1}(tr(\mathbf{o}) - 1)]\Big|\kappa\right), \quad \mathbf{o} \in \Omega.$$

That is, with probability space $(\Omega, \mathcal{F}, F)$ and $A \in \mathcal{F}$,

$$P_F(\mathbf{O} \in A) = P_{F^*}((\tau, \phi, |r|) \in M^{-1}(A)) = \int_{(\tau,\phi,|r|)\in M^{-1}(A)} \frac{dF^*}{dH^*} dH^* = \int_{\mathbf{o}\in A} f(\mathbf{o}) dH$$

where $f(\mathbf{o}) = dF^*(M^{-1}(\mathbf{o}))/dH^*$ and $P_H(A) = P_{H^*}(M^{-1}(A))$.

More generally, a density for $\mathbf{O} \sim$ UARS($\mathbf{S}$, κ) is given by

$$f(\mathbf{o}|\mathbf{S}, \kappa) = \frac{4\pi}{3 - tr(\mathbf{S}^T\mathbf{o})} C\left(\arccos[2^{-1}(tr(\mathbf{S}^T\mathbf{o}) - 1)]\Big|\kappa\right), \quad \mathbf{o} \in \Omega,$$

with respect to H, which follows from $\mathbf{S}^T \cdot \mathbf{O} \sim$ UARS($\mathbf{I}_{3\times 3}$, κ) and the invariance of the Haar measure (i.e., $P_H(A) = P_H(\mathbf{S}^T A)$).

On-line Appendix B: Proofs of UARS Properties from the Main Paper's Appendix

In what follows, let $\mathbf{U} = (u, v, w)^T$ be uniformly distributed on the sphere, independently of $r \sim$ Circ(κ).

Proof of Property 1. Recall that $\mathbf{O} = M(\mathbf{U}, r) \sim \text{UARS}(\mathbf{I}_{3\times 3},\ \kappa)$ and note that $\mathbf{O}^T = M(-\mathbf{U}, r)$ by (2). Since $\mathbf{U}$ is uniformly distributed on the sphere and is independent of r, so is $-\mathbf{U}$. Thus, $\mathbf{O}^T = M(-\mathbf{U}, r) \stackrel{d}{=} M(\mathbf{U}, r) \sim \text{UARS}(\mathbf{I}_{3\times 3}, \kappa)$. □

Proof of Property 2. We note the matrix identity

$$\mathbf{S} \cdot M(\mathbf{U}, r) \cdot \mathbf{S}^T = M(\mathbf{S} \cdot \mathbf{U}, r)$$

can be proven by considering $\mathbf{S} = g(\alpha, \beta, \gamma)$ as in (8). Since $\mathbf{U}$ is uniform on the sphere and is independent of r, so is $\mathbf{S} \cdot \mathbf{U}$ and

$$\mathbf{O} = M(\mathbf{U}, r) \stackrel{d}{=} M(\mathbf{S} \cdot \mathbf{U}, r) = \mathbf{S} \cdot \mathbf{O} \cdot \mathbf{S}^T. \tag{B.1}$$

□

Proof of Property 3. By definition $\mathbf{S}\cdot\mathbf{O} \sim \text{UARS}(\mathbf{S}, \kappa)$. By (B.1), $\mathbf{O} \stackrel{d}{=} \mathbf{S}\cdot\mathbf{O}\cdot\mathbf{S}^T$. Multiplying by $\mathbf{S}$ on the right gives $\mathbf{O} \cdot \mathbf{S} \stackrel{d}{=} \mathbf{S} \cdot \mathbf{O} \sim \text{UARS}(\mathbf{S}, \kappa)$. □

Proof of Property 4. $\mathbf{S}^T \cdot \mathbf{O} \sim \text{UARS}(\mathbf{I}_{3\times 3}, \kappa)$ so that $\mathbf{O}^T \cdot \mathbf{S} \sim \text{UARS}(\mathbf{I}_{3\times 3}, \kappa)$ by Property 1. Then $\mathbf{O}^T = (\mathbf{O}^T \cdot \mathbf{S}) \cdot \mathbf{S}^T \sim \text{UARS}(\mathbf{S}^T, \kappa)$ by Property 3. □

Proof of Property 5. By definition $\mathbf{S}^T\cdot\mathbf{O} \sim \text{UARS}(\mathbf{I}_{3\times 3}, \kappa)$. By (B.1), $\mathbf{S}\cdot(\mathbf{S}^T\cdot\mathbf{O})\cdot\mathbf{S}^T \stackrel{d}{=} \mathbf{S}^T\cdot\mathbf{O}$. Thus $\mathbf{O} \cdot \mathbf{S}^T \sim \text{UARS}(\mathbf{I}_{3\times 3}, \kappa)$. □

Proof of Property 6. As in (B.1), $\mathbf{O} = M(\mathbf{U}, r) \stackrel{d}{=} M(\mathbf{Q}\mathbf{U}, r)$ for any 3×3 orthogonal rotation matrix $\mathbf{Q}$. Let

$$\mathbf{Q} = \begin{pmatrix} 0 & -1 & 0 \\ -1 & 0 & 0 \\ 0 & 0 & -1 \end{pmatrix}.$$

Then $\mathbf{Q}\mathbf{U} = (-v, -u, -w)^T$, and

$$M(\mathbf{Q}\mathbf{U}, r) = \begin{pmatrix} v^2 + (u^2 + w^2)\cos r & uv(1 - \cos r) + w \sin r & vw(1 - \cos r) - u \sin r \\ uv(1 - \cos r) - w \sin r & u^2 + (v^2 + w^2)\cos r & uw(1 - \cos r) + v \sin r \\ vw(1 - \cos r) + u \sin r & uw(1 - \cos r) - v \sin r & w^2 + (u^2 + v^2)\cos r \end{pmatrix}.$$

Now, to compare P_X with P_Y we must rotate $\mathbf{Y}$ to also be about the vector $(1,0,0)^T$. We can do this by taking $\mathbf{RY}$ where

$$\mathbf{R} = \begin{pmatrix} 0 & 1 & 0 \\ 1 & 0 & 0 \\ 0 & 0 & 1 \end{pmatrix}.$$

Thus, $\mathbf{RY} = (v^2+(u^2+w^2)\cos r,\ uv(1-\cos r)-w\sin r,\ vw(1-\cos r)+u\sin r)^T$ is distributed about $(1,0,0)^T$. But, $\mathbf{RY}$ is the same as the first column of $M(\mathbf{QU}, r) \stackrel{d}{=} M(\mathbf{U}, r) = \mathbf{O}$. Thus, $\mathbf{RY} \stackrel{d}{=} \mathbf{X}$ and $P_X = P_Y$. The fact that $P_Y = P_Z$ can be established in a similar manner by using

$$\mathbf{Q} = \begin{pmatrix} -1 & 0 & 0 \\ 0 & 0 & -1 \\ 0 & -1 & 0 \end{pmatrix} \text{ and } \mathbf{R} = \begin{pmatrix} 1 & 0 & 0 \\ 0 & 0 & 1 \\ 0 & 1 & 0 \end{pmatrix}. \qquad \square$$

Proof of Property 7. We write $\mathbf{O} = M(\mathbf{U}, r)$ for $\mathbf{U}$ uniformly distributed on the sphere. Expressing $\mathbf{U}$ in terms of θ and ϕ as in (1), and using the fact that θ, ϕ, and r are independently distributed, we have $\mathrm{E}(uv) = \mathrm{E}(uw) = \mathrm{E}(vw) = 0$, $\mathrm{E}(u^2) = \mathrm{E}(v^2) = \mathrm{E}(w^2) = \frac{1}{3}$, $\mathrm{E}(\sin r) = 0$, and $\mathrm{E}(\cos r) = \frac{I_1(\kappa)}{I_0(\kappa)}$. The first expectation follows.

Now, for $j_1, j_2, j_3, j_4 \in \{1,2,3\}$, we find

$$\mathrm{E}(O_{j_1 j_2}^2) = \begin{cases} \dfrac{1}{5} + \dfrac{4}{15}\cdot\dfrac{I_1(\kappa)}{I_0(\kappa)} + \dfrac{8}{15}\cdot\dfrac{I_2(\kappa)+\frac{1}{\kappa}I_1(\kappa)}{I_0(\kappa)} & \text{for } j_1 = j_2 \\ \dfrac{1}{15} + \dfrac{I_2(\kappa)+(\frac{1}{\kappa}-2)I_1(\kappa)}{15I_0(\kappa)} + \dfrac{I_1(\kappa)}{3\kappa I_0(\kappa)} & \text{for } j_1 \neq j_2 \end{cases},$$

$$\mathrm{E}(O_{12}O_{21}) = \mathrm{E}(O_{23}O_{32}) = \mathrm{E}(O_{13}O_{31}) = \frac{1}{15} + \frac{I_2(\kappa)+(\frac{1}{\kappa}-2)I_1(\kappa)}{15I_0(\kappa)} - \frac{I_1(\kappa)}{3\kappa I_0(\kappa)},$$

and

$$\mathrm{E}(O_{11}O_{22}) = \mathrm{E}(O_{11}O_{33}) = \mathrm{E}(O_{22}O_{33}) = \frac{1}{15} + \frac{8}{15}\cdot\frac{I_1(\kappa)}{I_0(\kappa)} + \frac{2}{5}\cdot\frac{I_2(\kappa)+\frac{1}{\kappa}I_1(\kappa)}{I_0(\kappa)},$$

while all other terms of the form $\mathrm{E}(O_{j_1j_2}O_{j_3j_4})$ are zero.

Let $\mathbf{P} = \mathbf{O}^2$. Then

$$\begin{aligned}\mathrm{E}(P_{11}) = \mathrm{E}(O_{11}^2 + O_{12}O_{21} + O_{13}O_{31}) &= \frac{1}{3} + \frac{2}{3}\left(\frac{I_2(\kappa) + \frac{1}{\kappa}I_1(\kappa)}{I_0(\kappa)} - \frac{I_1(\kappa)}{\kappa I_0(\kappa)}\right) \\ &= \frac{1}{3} + \frac{2}{3}\frac{I_2(\kappa)}{I_0(\kappa)}.\end{aligned}$$

Finding all other entries of $\mathbf{P}$ in a similar manner gives $\mathrm{E}(P_{22}) = \mathrm{E}(P_{33}) = \mathrm{E}(P_{11})$ and $\mathrm{E}(P_{ij}) = 0$ for all $i, j \in \{1, 2, 3\}$, $i \neq j$. The second expectation follows. □

Proof of Property 8. First, we have that $x = O_{11}$, $y = O_{22}$, and $z = O_{33}$. From the proof of Property 7,

$$\mathrm{E}(O_{11}O_{22}) = \mathrm{E}(O_{11}O_{33}) = \mathrm{E}(O_{22}O_{33}) = \frac{1}{15} + \frac{8}{15} \cdot \frac{I_1(\kappa)}{I_0(\kappa)} + \frac{2}{5} \cdot \frac{I_2(\kappa) + \frac{1}{\kappa}I_1(\kappa)}{I_0(\kappa)}$$

and

$$\mathrm{E}(O_{11}^2) = \mathrm{E}(O_{22}^2) = \mathrm{E}(O_{33}^2) = \frac{1}{5} + \frac{4}{15} \cdot \frac{I_1(\kappa)}{I_0(\kappa)} + \frac{8}{15} \cdot \frac{I_2(\kappa) + \frac{1}{\kappa}I_1(\kappa)}{I_0(\kappa)}.$$

Also, by Property 7,

$$\mathrm{E}(O_{11}) = \mathrm{E}(O_{22}) = \mathrm{E}(O_{33}) = \frac{1}{3} + \frac{2}{3}\frac{I_1(\kappa)}{I_0(\kappa)}.$$

Therefore, the result follows. □

Proof of Property 9. Since $\mathbf{O} \sim$ vM-UARS($\mathbf{S}$, κ), we can write $\mathbf{O} = \mathbf{S} \cdot \mathbf{P}$ where $\mathbf{P} \sim$ vM-UARS($\mathbf{I}_{3\times3}$, κ) and $\mathbf{S} = g(\alpha, \beta, \gamma)$ as in (8). Now, by Property 7,

$$\mathrm{E}(\mathbf{O}) = \mathrm{E}(\mathbf{S} \cdot \mathbf{P}) = \mathbf{S} \cdot \mathrm{E}(\mathbf{P}) = \left(\frac{1}{3} + \frac{2}{3}\frac{I_1(\kappa)}{I_0(\kappa)}\right) \cdot \mathbf{S}.$$

Then,

$$\begin{aligned}\mathrm{E}\left(\frac{\partial l}{\partial \kappa}\right) &= \mathrm{E}\left(\frac{1}{2}\left[P_{11} + P_{22} + P_{33} - 1\right] - \frac{I_1(\kappa)}{I_0(\kappa)}\right) \\ &= \frac{1}{2}\left[3\left(\frac{1}{3} + \frac{2}{3}\frac{I_1(\kappa)}{I_0(\kappa)}\right) - 1\right] - \frac{I_1(\kappa)}{I_0(\kappa)} = 0\end{aligned}$$

and

$$\mathrm{E}\left(\frac{\partial l}{\partial \alpha}\right) \;=\; \frac{\kappa}{2}\,\mathrm{E}\left(\frac{\partial P_{11}}{\partial \alpha}+\frac{\partial P_{22}}{\partial \alpha}+\frac{\partial P_{33}}{\partial \alpha}\right)$$

where

$$\begin{aligned} P_{11} &= s_{11}\cdot O_{11}+s_{21}\cdot O_{21}+s_{31}\cdot O_{31} \\ P_{22} &= s_{12}\cdot O_{12}+s_{22}\cdot O_{22}+s_{32}\cdot O_{32} \\ P_{33} &= s_{13}\cdot O_{13}+s_{23}\cdot O_{23}+s_{33}\cdot O_{33} \end{aligned} \tag{B.2}$$

and s_{ij} are the elements of $\mathbf{S}$. By calculating each of the partial derivatives, we find that

$$\begin{aligned} \mathrm{E}\left(\frac{\partial l}{\partial \alpha}\right) &= \frac{\kappa}{2}\,\mathrm{E}\left(-s_{12}\cdot O_{11}-s_{22}\cdot O_{21}-s_{32}\cdot O_{31}+s_{11}\cdot O_{12}+s_{21}\cdot O_{22}+s_{31}\cdot O_{32}\right) \\ &= \frac{\kappa}{2}\left(\frac{1}{3}+\frac{2}{3}\frac{I_1(\kappa)}{I_0(\kappa)}\right)\left(-s_{12}s_{11}-s_{22}s_{21}-s_{32}s_{31}+s_{11}s_{12}+s_{21}s_{22}+s_{31}s_{32}\right) \;=\; 0. \end{aligned}$$

In a similar manner it can be shown that $\mathrm{E}\left(\frac{\partial l}{\partial \beta}\right)=0$ and $\mathrm{E}\left(\frac{\partial l}{\partial \gamma}\right)=0$. □

Proof of Property 10. Again, since $\mathbf{O}\sim$ vM-UARS($\mathbf{S}$, κ), we can write $\mathbf{O}=\mathbf{S}\cdot\mathbf{P}$ where $\mathbf{P}\sim$ vM-UARS($\mathbf{I}_{3\times 3}$, κ). As in the proof of Property 9, $\mathrm{E}(\mathbf{O})=D(\kappa)\cdot\mathbf{S}$. Now, we must calculate $l''(\kappa,(\alpha,\beta,\gamma))$. First, we note that

$$\frac{\partial^2 l}{\partial \kappa^2}=-\frac{I_2(\kappa)+\frac{1}{\kappa}I_1(\kappa)}{I_0(\kappa)}+\left(\frac{I_1(\kappa)}{I_0(\kappa)}\right)^2.$$

Second, let $\eta,\psi\in\{\alpha,\beta,\gamma\}$. Then,

$$\frac{\partial^2 l}{\partial \kappa\partial \eta}=\frac{1}{2}\left(\frac{\partial P_{11}}{\partial \eta}+\frac{\partial P_{22}}{\partial \eta}+\frac{\partial P_{33}}{\partial \eta}\right)$$

and

$$\frac{\partial^2 l}{\partial \eta\partial \psi}=\frac{\kappa}{2}\left(\frac{\partial^2 P_{11}}{\partial \eta\partial \psi}+\frac{\partial^2 P_{22}}{\partial \eta\partial \psi}+\frac{\partial^2 P_{33}}{\partial \eta\partial \psi}\right), \tag{B.3}$$

where P_{11}, P_{22}, and P_{33} are as in (B.2).

We will provide the details of finding $\mathrm{E}\left(\frac{\partial^2 l}{\partial \alpha\partial \gamma}\right)$ and leave the other terms to the reader. By (B.3),

$$\mathrm{E}\left(\frac{\partial^2 l}{\partial \alpha\partial \gamma}\right)=\frac{\kappa}{2}\left[\mathrm{E}\left(\frac{\partial^2 P_{11}}{\partial \alpha\partial \gamma}\right)+\mathrm{E}\left(\frac{\partial^2 P_{22}}{\partial \alpha\partial \gamma}\right)+\mathrm{E}\left(\frac{\partial^2 P_{33}}{\partial \alpha\partial \gamma}\right)\right].$$

Now,

$$\mathrm{E}\left(\frac{\partial^2 P_{11}}{\partial\alpha\partial\gamma}\right) = -s_{22}\cdot\mathrm{E}(O_{11}) + s_{12}\cdot\mathrm{E}(O_{21}) + 0\cdot\mathrm{E}(O_{31}) = (-s_{22}s_{11} + s_{12}s_{21})\,D(\kappa),$$
$$\mathrm{E}\left(\frac{\partial^2 P_{22}}{\partial\alpha\partial\gamma}\right) = s_{21}\cdot\mathrm{E}(O_{12}) - s_{11}\cdot\mathrm{E}(O_{22}) + 0\cdot\mathrm{E}(O_{32}) = (s_{21}s_{12} - s_{11}s_{22})\,D(\kappa),$$

and

$$\mathrm{E}\left(\frac{\partial^2 P_{33}}{\partial\alpha\partial\gamma}\right) = 0.$$

Thus,

$$\mathrm{E}\left(\frac{\partial^2 l}{\partial\alpha\partial\gamma}\right) = \frac{\kappa}{2}\left[2(s_{12}s_{21} - s_{11}s_{22})D(\kappa)\right] = \kappa(s_{12}s_{21} - s_{11}s_{22})D(\kappa).$$

Now,

$$\begin{aligned}
s_{12}s_{21} - s_{11}s_{22} &= (\sin\alpha\cos\gamma + \cos\alpha\sin\gamma\cos\beta)(-\cos\alpha\sin\gamma - \sin\alpha\cos\gamma\cos\beta) \\
&\quad -(\cos\alpha\cos\gamma - \sin\alpha\sin\gamma\cos\beta)(-\sin\alpha\sin\gamma + \cos\alpha\cos\gamma\cos\beta) \\
&= -(\cos^2\alpha\sin^2\gamma + \sin^2\alpha\cos^2\gamma + \sin^2\alpha\sin^2\gamma + \cos^2\alpha\cos^2\gamma)\cos\beta \\
&= -\cos\beta
\end{aligned}$$

Therefore,

$$-\mathrm{E}\left(\frac{\partial^2 l}{\partial\alpha\partial\gamma}\right) = \kappa\cos\beta\cdot D(\kappa). \qquad \square$$

Proof of Property 11. By Property 9, $\mathrm{Var}(l'(\kappa,(\alpha,\beta,\gamma)) = \mathrm{E}(l'(\kappa,(\alpha,\beta,\gamma))^2)$. Again, since $\mathbf{O}\sim$ vM-UARS($\mathbf{S}$, κ), we can write $\mathbf{O} = \mathbf{S}\cdot\mathbf{P}$ where $\mathbf{P}\sim$ vM-UARS($\mathbf{I}_{3\times3}$, κ). Recall that we can express $\mathbf{P}$ as $\mathbf{P} = M(\mathbf{U}, r)$ and in the proof of Property 7 we found $\mathrm{E}(P_{j_1j_2}P_{j_3j_4})$ for all $j_1, j_2, j_3, j_4 \in \{1,2,3\}$.

We present the details required for finding just one term of $\mathrm{E}(l'(\kappa,(\alpha,\beta,\gamma))^2)$. Others may be found similarly. We will calculate $\mathrm{E}\left(\left(\frac{\partial l}{\partial\alpha}\right)^2\right)$.

First,

$$\mathrm{E}\left(\left(\frac{\partial l}{\partial\alpha}\right)^2\right) = \frac{\kappa^2}{4}\,\mathrm{E}\left(\left(\frac{\partial P_{11}}{\partial\alpha} + \frac{\partial P_{22}}{\partial\alpha} + \frac{\partial P_{33}}{\partial\alpha}\right)^2\right),$$

where P_{11}, P_{22}, and P_{33} are as in (B.2). Using the proof of Property 9,

$$\mathrm{E}\left(\left(\frac{\partial l}{\partial\alpha}\right)^2\right) = \frac{\kappa^2}{4}\,\mathrm{E}\left((-s_{12}\cdot O_{11} - s_{22}\cdot O_{21} - s_{32}\cdot O_{31} + s_{11}\cdot O_{12} + s_{21}\cdot O_{22} + s_{31}\cdot O_{32})^2\right).$$

Expanding, we have

$$\begin{aligned}
\mathrm{E}\left(\left(\frac{\partial l}{\partial \alpha}\right)^2\right) &= \frac{\kappa^2}{4}\left(s_{12}^2\mathrm{E}(O_{11}^2) + s_{22}^2\mathrm{E}(O_{21}^2) + s_{32}^2\mathrm{E}(O_{31}^2)\right. \\
&\quad + s_{11}^2\mathrm{E}(O_{12}^2) + s_{21}^2\mathrm{E}(O_{22}^2) + s_{31}^2\mathrm{E}(O_{32}^2) \\
&\quad + 2s_{12}s_{22}\mathrm{E}(O_{11}O_{21}) + 2s_{12}s_{32}\mathrm{E}(O_{11}O_{31}) - 2s_{12}s_{11}\mathrm{E}(O_{11}O_{12}) \\
&\quad - 2s_{12}s_{21}\mathrm{E}(O_{11}O_{22}) - 2s_{12}s_{31}\mathrm{E}(O_{11}O_{32}) + 2s_{22}s_{32}\mathrm{E}(O_{21}O_{31}) \\
&\quad - 2s_{22}s_{11}\mathrm{E}(O_{21}O_{12}) - 2s_{22}s_{21}\mathrm{E}(O_{21}O_{22}) - 2s_{22}s_{31}\mathrm{E}(O_{21}O_{32}) \\
&\quad - 2s_{32}s_{11}\mathrm{E}(O_{31}O_{12}) - 2s_{32}s_{21}\mathrm{E}(O_{31}O_{22}) - 2s_{32}s_{31}\mathrm{E}(O_{31}O_{32}) \\
&\quad + 2s_{11}s_{21}\mathrm{E}(O_{12}O_{22}) + 2s_{11}s_{31}\mathrm{E}(O_{12}O_{32}) \\
&\quad \left. + 2s_{21}s_{31}\mathrm{E}(O_{22}O_{32})\right). \qquad \text{(B.4)}
\end{aligned}$$

Now, for any $j, k \in \{1, 2, 3\}$,

$$\begin{aligned}
\mathrm{E}(O_{j1}O_{k2}) &= \mathrm{E}((s_{j1}P_{11} + s_{j2}P_{21} + s_{j3}P_{31})(s_{k1}P_{12} + s_{k2}P_{22} + s_{k3}P_{32})) \\
&= s_{j2}s_{k1}\mathrm{E}(P_{21}P_{12}) + s_{j1}s_{k2}\mathrm{E}(P_{11}P_{22}), \\
\mathrm{E}(O_{j1}O_{k1}) &= s_{j1}s_{k1}\mathrm{E}(P_{11}^2) + s_{j2}s_{k2}\mathrm{E}(P_{21}^2) + s_{j3}s_{k3}\mathrm{E}(P_{31}^2) \\
\mathrm{E}(O_{j2}O_{k2}) &= s_{j1}s_{k1}\mathrm{E}(P_{12}^2) + s_{j2}s_{k2}\mathrm{E}(P_{22}^2) + s_{j3}s_{k3}\mathrm{E}(P_{32}^2) \qquad \text{(B.5)}
\end{aligned}$$

By placing the quantities from (B.5) into (B.4) and simplifying, we find

$$\begin{aligned}
\mathrm{E}\left(\left(\frac{\partial l}{\partial \alpha}\right)^2\right) &= \frac{\kappa^2}{4}(\mathrm{E}(P_{11}^2)(s_{11}s_{12}+s_{21}s_{22}+s_{31}s_{32})^2+\mathrm{E}(P_{21}^2)(s_{12}^2+s_{22}^2+s_{32}^2)^2 \\
&\quad +\mathrm{E}(P_{31}^2)(s_{13}s_{12}+s_{23}s_{22}+s_{33}s_{32})^2+\mathrm{E}(P_{12}^2)(s_{11}^2+s_{21}^2+s_{31}^2)^2 \\
&\quad +\mathrm{E}(P_{22}^2)(s_{12}s_{11}+s_{22}s_{21}+s_{32}s_{31})^2 \\
&\quad +\mathrm{E}(P_{32}^2)(s_{13}s_{11}+s_{23}s_{21}+s_{33}s_{31})^2 \\
&\quad -2\mathrm{E}(P_{21}P_{12})(s_{11}^2+s_{21}^2+s_{31}^2)(s_{12}^2+s_{22}^2+s_{32}^2) \\
&\quad -2\mathrm{E}(P_{11}P_{22})(s_{11}s_{12}+s_{21}s_{22}+s_{31}s_{32})^2) \\
&= \frac{\kappa^2}{4}(\mathrm{E}(P_{21}^2)+\mathrm{E}(P_{12}^2)-2\mathrm{E}(P_{21}P_{12})) \\
&= \frac{\kappa^2}{4}\left(\frac{4I_1(\kappa)}{3\kappa I_0(\kappa)}\right) \\
&= \frac{\kappa I_1(\kappa)}{3I_0(\kappa)}.
\end{aligned}$$

□

On-line Appendix C: Proofs of Propositions from Section 3.3

Proof of Proposition 1. By Taylor expansion we have

$$0 = l_n'(\hat{\boldsymbol{\theta}}_n) \approx l_n'(\boldsymbol{\theta}_0) + l_n''(\boldsymbol{\theta}_0)(\hat{\boldsymbol{\theta}}_n - \boldsymbol{\theta}_0)$$

Since $\frac{1}{\sqrt{n}} l_n'(\boldsymbol{\theta}_0) \xrightarrow{d} \mathrm{MVN}(\mathbf{0}, \mathcal{I}_1(\boldsymbol{\theta}_0))$ and $-\frac{1}{n} l_n''(\boldsymbol{\theta}_0) \xrightarrow{p} H_1(\boldsymbol{\theta}_0)$, (positive definite), we have

$$\sqrt{n}(\hat{\boldsymbol{\theta}}_n - \boldsymbol{\theta}_0) \approx \left[\frac{-l_n''(\boldsymbol{\theta}_0)}{n}\right]^{-1} \frac{1}{\sqrt{n}} l_n'(\boldsymbol{\theta}_0) \xrightarrow{d} \mathrm{MVN}(\mathbf{0}, H_1^{-1}(\boldsymbol{\theta}_0)\mathcal{I}_1(\boldsymbol{\theta}_0)H_1^{-1}(\boldsymbol{\theta_0})). \tag{C.1}$$

□

Proof of Proposition 2. First we write $-2\log(\lambda_n) = 2\left[l_n(\hat{\boldsymbol{\theta}}_n) - l_n(\boldsymbol{\theta}_n^*)\right]$ where $\hat{\boldsymbol{\theta}}_n$ is the maximum quasi-likelihood estimate over Θ and $\boldsymbol{\theta}_n^*$ is the maximum quasi-likelihood estimate over Θ_0. By a Taylor expansion of $l_n(\boldsymbol{\theta}_n^*)$ about $\hat{\boldsymbol{\theta}}_n$, we get

$$l_n(\boldsymbol{\theta}_n^*) \approx l_n(\hat{\boldsymbol{\theta}}_n) + l_n'(\hat{\boldsymbol{\theta}}_n)(\boldsymbol{\theta}_n^* - \hat{\boldsymbol{\theta}}_n) + \frac{1}{2}(\boldsymbol{\theta}_n^* - \hat{\boldsymbol{\theta}}_n)^T l_n''(\hat{\boldsymbol{\theta}}_n)(\boldsymbol{\theta}_n^* - \hat{\boldsymbol{\theta}}_n)$$

Now, $-\frac{1}{n}l_n''(\hat{\boldsymbol{\theta}}_n) \xrightarrow{p} H_1(\boldsymbol{\theta}_0)$ and, since $\hat{\boldsymbol{\theta}}_n$ is the maximum quasi-likelihood estimate over Θ, $l_n'(\hat{\boldsymbol{\theta}}_n) = 0$. So,

$$\begin{aligned} 2\left[l_n(\hat{\boldsymbol{\theta}}_n) - l_n(\boldsymbol{\theta}_n^*)\right] &\approx -2\, l_n'(\hat{\boldsymbol{\theta}}_n)(\boldsymbol{\theta}_n^* - \hat{\boldsymbol{\theta}}_n) - (\boldsymbol{\theta}_n^* - \hat{\boldsymbol{\theta}}_n)^T l_n''(\hat{\boldsymbol{\theta}}_n)(\boldsymbol{\theta}_n^* - \hat{\boldsymbol{\theta}}_n) \\ &\approx n(\boldsymbol{\theta}_n^* - \hat{\boldsymbol{\theta}}_n)^T \left[-\frac{1}{n} l_n''(\hat{\boldsymbol{\theta}}_n)\right](\boldsymbol{\theta}_n^* - \hat{\boldsymbol{\theta}}_n) \\ &\approx n(\boldsymbol{\theta}_n^* - \hat{\boldsymbol{\theta}}_n)^T H_1(\boldsymbol{\theta}_0)(\boldsymbol{\theta}_n^* - \hat{\boldsymbol{\theta}}_n). \end{aligned} \tag{C.2}$$

Next, we expand $l_n'(\boldsymbol{\theta}_n^*)$ about $\hat{\boldsymbol{\theta}}_n$ giving

$$\frac{1}{\sqrt{n}} l_n'(\boldsymbol{\theta}_n^*) \approx \frac{1}{\sqrt{n}} l_n'(\hat{\boldsymbol{\theta}}_n) + \frac{1}{n} l_n''(\hat{\boldsymbol{\theta}}_n)\sqrt{n}(\boldsymbol{\theta}_n^* - \hat{\boldsymbol{\theta}}_n),$$

or

$$\sqrt{n}(\boldsymbol{\theta}_n^* - \hat{\boldsymbol{\theta}}_n) \approx \left[\frac{1}{n} l_n''(\hat{\boldsymbol{\theta}}_n)\right]^{-1} \frac{1}{\sqrt{n}} l_n'(\boldsymbol{\theta}_n^*) \approx -H_1^{-1}(\boldsymbol{\theta}_0) \frac{1}{\sqrt{n}} l_n'(\boldsymbol{\theta}_n^*).$$

By (C.2)

$$-2\log(\lambda_n) \approx \frac{1}{\sqrt{n}} l_n'(\boldsymbol{\theta}_n^*) H_1^{-1}(\boldsymbol{\theta}_0) \frac{1}{\sqrt{n}} l_n'(\boldsymbol{\theta}_n^*). \tag{C.3}$$

Now, we expand $l_n'(\boldsymbol{\theta}_n^*)$ about $\boldsymbol{\theta}_0$, yielding

$$\begin{aligned} \frac{1}{\sqrt{n}} l_n'(\boldsymbol{\theta}_n^*) &\approx \frac{1}{\sqrt{n}} l_n'(\boldsymbol{\theta}_0) + \frac{1}{n} l_n''(\boldsymbol{\theta}_0)\sqrt{n}(\boldsymbol{\theta}_n^* - \boldsymbol{\theta}_0) \\ &\approx \frac{1}{\sqrt{n}} l_n'(\boldsymbol{\theta}_0) - H_1(\boldsymbol{\theta}_0)\sqrt{n}(\boldsymbol{\theta}_n^* - \boldsymbol{\theta}_0). \end{aligned} \tag{C.4}$$

Now, partition $H_1(\boldsymbol{\theta}_0)$ into $H_1(\boldsymbol{\theta}_0) = \begin{bmatrix} \mathbf{G}_1 & \mathbf{G}_2 \\ \mathbf{G}_2^T & \mathbf{G}_3 \end{bmatrix}$ where $\mathbf{G}_1$ is $r \times r$ and let $\mathbf{J} = \begin{bmatrix} \mathbf{0} & \mathbf{0} \\ \mathbf{0} & \mathbf{G}_3^{-1} \end{bmatrix}$.

Since $\boldsymbol{\theta}_n^*$ is the maximum quasi-likelihood estimate over Θ_0, we have $\boldsymbol{\theta}_n^* = \begin{pmatrix} \boldsymbol{\theta}_{01} \\ \boldsymbol{\theta}_2^* \end{pmatrix}$ where $\boldsymbol{\theta}_2^*$ maximizes the quasi-likelihood under the restriction that $\boldsymbol{\theta}_1 = \boldsymbol{\theta}_{01}$. Thus, the last $4 - r$ components of $l_n'(\boldsymbol{\theta}_n^*)$ are 0, so that $\mathbf{J} \cdot l_n'(\boldsymbol{\theta}_n^*) = 0$. Then, by (C.4),

$$\frac{1}{\sqrt{n}} \mathbf{J} \cdot l_n'(\boldsymbol{\theta}_n^*) \approx \frac{1}{\sqrt{n}} \mathbf{J} \cdot l_n'(\boldsymbol{\theta}_0) - \mathbf{J} H_1(\boldsymbol{\theta}_0)\sqrt{n}(\boldsymbol{\theta}_n^* - \boldsymbol{\theta}_0),$$

implying that

$$\frac{1}{\sqrt{n}} \mathbf{J} \cdot l_n'(\boldsymbol{\theta}_0) \approx \mathbf{J} H_1(\boldsymbol{\theta}_0)\sqrt{n}(\boldsymbol{\theta}_n^* - \boldsymbol{\theta}_0) = \sqrt{n}(\boldsymbol{\theta}_n^* - \boldsymbol{\theta}_0),$$

which follows from $(\boldsymbol{\theta}_n^* - \boldsymbol{\theta}_0) = \begin{pmatrix} \mathbf{0} \\ \boldsymbol{\theta}_2^* - \boldsymbol{\theta}_{02} \end{pmatrix}$ and $\mathbf{J}H_1(\boldsymbol{\theta}_0) = \begin{bmatrix} \mathbf{0} & \mathbf{0} \\ \mathbf{G}_3^{-1}\mathbf{G}_2^T & \mathbf{I}_{3\times 3} \end{bmatrix}$ so that $\mathbf{J}H_1(\boldsymbol{\theta}_0)\sqrt{n}(\boldsymbol{\theta}_n^* - \boldsymbol{\theta}_0) = \sqrt{n}\begin{pmatrix} \mathbf{0} \\ \boldsymbol{\theta}_2^* - \boldsymbol{\theta}_{02} \end{pmatrix} = \sqrt{n}(\boldsymbol{\theta}_n^* - \boldsymbol{\theta}_0)$. Thus, by (C.4),

$$\frac{1}{\sqrt{n}}l_n'(\boldsymbol{\theta}_n^*) \approx \frac{1}{\sqrt{n}}l_n'(\boldsymbol{\theta}_0) - H_1(\boldsymbol{\theta}_0)\mathbf{J}\frac{1}{\sqrt{n}}l_n'(\boldsymbol{\theta}_0) = [\mathbf{I}_{3\times 3} - H_1(\boldsymbol{\theta}_0)J]\frac{1}{\sqrt{n}}l_n'(\boldsymbol{\theta}_0). \tag{C.5}$$

By the Central Limit Theorem, $\frac{1}{\sqrt{n}}l_n'(\boldsymbol{\theta}_0) \xrightarrow{d} \mathbf{Y}$ where $\mathbf{Y} \sim \text{MVN}(\mathbf{0}, \mathcal{I}_1(\boldsymbol{\theta}_0))$. Therefore, by (C.3) and (C.5), we have

$$\begin{aligned} -2\log(\lambda_n) &\xrightarrow{d} \mathbf{Y}^T[\mathbf{I}_{3\times 3} - H_1(\boldsymbol{\theta}_0)\mathbf{J}]^T H_1^{-1}(\boldsymbol{\theta}_0)[\mathbf{I}_{3\times 3} - H_1(\boldsymbol{\theta}_0)\mathbf{J}]\mathbf{Y} \\ &= \mathbf{Y}^T[\mathbf{I}_{3\times 3} - \mathbf{J}H_1(\boldsymbol{\theta}_0)]H_1^{-1}(\boldsymbol{\theta}_0)[\mathbf{I}_{3\times 3} - H_1(\boldsymbol{\theta}_0)\mathbf{J}]\mathbf{Y} \\ &= \mathbf{Y}^T[H_1^{-1}(\boldsymbol{\theta}_0) - \mathbf{J}][\mathbf{I}_{3\times 3} - H_1(\boldsymbol{\theta}_0)\mathbf{J}]\mathbf{Y} \\ &= \mathbf{Y}^T[H_1^{-1}(\boldsymbol{\theta}_0) - 2\mathbf{J} + \mathbf{J}H_1(\boldsymbol{\theta}_0)\mathbf{J}]\mathbf{Y} \end{aligned}$$

Now,

$$\mathbf{J}H(\boldsymbol{\theta}_0)\mathbf{J} = \begin{bmatrix} \mathbf{0} & \mathbf{0} \\ \mathbf{0} & \mathbf{G}_3^{-1} \end{bmatrix}\begin{bmatrix} \mathbf{G}_1 & \mathbf{G}_2 \\ \mathbf{G}_2^T & \mathbf{G}_3 \end{bmatrix}\begin{bmatrix} \mathbf{0} & \mathbf{0} \\ \mathbf{0} & \mathbf{G}_3^{-1} \end{bmatrix} = \begin{bmatrix} \mathbf{0} & \mathbf{0} \\ \mathbf{0} & \mathbf{G}_3^{-1} \end{bmatrix} = \mathbf{J},$$

giving $-2\log(\lambda_n) \xrightarrow{d} \mathbf{Y}^T[H_1^{-1}(\boldsymbol{\theta}_0) - \mathbf{J}]\mathbf{Y}$. Let $\mathbf{Z} = \mathcal{I}_1(\boldsymbol{\theta}_0)^{-\frac{1}{2}}\mathbf{Y}$. Then, $\mathbf{Z} \sim \text{MVN}(\mathbf{0}, \mathbf{I}_{3\times 3})$ and

$$\begin{aligned} -2\log(\lambda_n) &\xrightarrow{d} \mathbf{Z}^T\mathcal{I}_1(\boldsymbol{\theta}_0)^{\frac{1}{2}}[H_1^{-1}(\boldsymbol{\theta}_0) - \mathbf{J}]\mathcal{I}_1(\boldsymbol{\theta}_0)^{\frac{1}{2}}\mathbf{Z} \\ &= \mathbf{Z}^T P(\boldsymbol{\theta}_0)\mathbf{Z}, \text{ where } P(\boldsymbol{\theta}_0) = \mathcal{I}_1(\boldsymbol{\theta}_0)^{\frac{1}{2}}[H_1^{-1}(\boldsymbol{\theta}_0) - \mathbf{J}]\mathcal{I}_1(\boldsymbol{\theta}_0)^{\frac{1}{2}}. \end{aligned}$$

Now, it can be calculated that

$$P(\boldsymbol{\theta}_0) = \begin{cases} \text{diag}\,(1, B(\kappa_0), B(\kappa_0), B(\kappa_0)) & \text{for} \quad \boldsymbol{\theta}_1 = \boldsymbol{\theta} \\ \text{diag}\,(0, B(\kappa_0), B(\kappa_0), B(\kappa_0)) & \text{for} \quad \boldsymbol{\theta}_1^T = (\alpha, \beta, \gamma) \\ \text{diag}\,(1, 0, 0, 0) & \text{for} \quad \boldsymbol{\theta}_1 = \kappa \end{cases}.$$

Therefore,

$$-2\log(\lambda_n) \xrightarrow{d} \begin{cases} \chi_1^2 + B(\kappa_0)\chi_3^2 & \text{for} \quad \boldsymbol{\theta}_1 = \boldsymbol{\theta} \\ B(\kappa_0)\chi_3^2 & \text{for} \quad \boldsymbol{\theta}_1^T = (\alpha, \beta, \gamma) \\ \chi_1^2 & \text{for} \quad \boldsymbol{\theta}_1 = \kappa \end{cases}. \qquad \square$$

Proof of Proposition 3. This follows directly from Proposition 1 that states

$$\sqrt{n}(\hat{\boldsymbol{\theta}}_n - \boldsymbol{\theta}_0) \xrightarrow{d} \text{MVN}(0, H_1^{-1}(\boldsymbol{\theta}_0)\mathcal{I}_1(\boldsymbol{\theta}_0)H_1^{-1}(\boldsymbol{\theta}_0)). \qquad \square$$

Proof of Proposition 4. By expanding $l_n'(\boldsymbol{\theta}_0)$ about $\tilde{\boldsymbol{\theta}}_n$, we have

$$\begin{aligned} \frac{1}{\sqrt{n}} l_n'(\boldsymbol{\theta}_0) &\approx \frac{1}{\sqrt{n}} l_n'(\tilde{\boldsymbol{\theta}}_n) + \frac{1}{n} l_n''(\tilde{\boldsymbol{\theta}}_n)\sqrt{n}(\boldsymbol{\theta}_0 - \tilde{\boldsymbol{\theta}}_n) \\ &\xrightarrow{d} \text{MVN}(\mathbf{0}, \mathcal{I}_1(\boldsymbol{\theta}_0)) + \mathcal{I}_1(\boldsymbol{\theta}_0)^{\frac{1}{2}}\boldsymbol{\delta} \end{aligned}$$

Let $\mathbf{Y} \sim \text{MVN}(\mathcal{I}_1(\boldsymbol{\theta}_0)^{\frac{1}{2}}\boldsymbol{\delta}, \mathcal{I}_1(\boldsymbol{\theta}_0))$. By modifying the proof of Proposition 2, we have

$$\begin{aligned} -2\log(\lambda_n) &\xrightarrow{d} \mathbf{Y}^T[H_1^{-1}(\boldsymbol{\theta}_0) - \mathbf{J}]\mathbf{Y} \\ &= \mathbf{Z}^T\mathcal{I}_1(\boldsymbol{\theta}_0)^{\frac{1}{2}}[H_1^{-1}(\boldsymbol{\theta}_0) - \mathbf{J}]\mathcal{I}_1(\boldsymbol{\theta}_0)^{\frac{1}{2}}\mathbf{Z} \text{ where } \mathbf{Z} = \mathcal{I}_1(\boldsymbol{\theta}_0)^{-\frac{1}{2}}\mathbf{Y} \\ &= \mathbf{Z}^T P(\boldsymbol{\theta}_0)\mathbf{Z}, \end{aligned}$$

where $P(\boldsymbol{\theta}_0) = \text{diag}\,(1, B(\kappa_0), B(\kappa_0), B(\kappa_0))$ and

$$\mathbf{Z}^T = (Z_1,\ Z_2,\ Z_3,\ Z_4) \sim \text{MVN}(\boldsymbol{\delta}, \mathbf{I}_{4\times 4}).$$

Now

$$\mathbf{Z}^T P(\boldsymbol{\theta}_0)\mathbf{Z} = Z_1^2 + B(\kappa_0)(Z_2^2 + Z_3^2 + Z_4^2)$$

and $Z_1^2 \sim \chi_1^2(\delta_\kappa^2)$ and $Z_2^2 + Z_3^2 + Z_4^2 \sim \chi_3^2(\delta_\alpha^2 + \delta_\beta^2 + \delta_\gamma^2)$ are independent. $\square$

Proof of Proposition 5. As in the proof of Proposition 4, $\frac{1}{\sqrt{n}} l_n'(\boldsymbol{\theta}_0) \xrightarrow{d} \mathbf{Y}$, where

$$\mathbf{Y} \sim \text{MVN}(H_1(\boldsymbol{\theta}_0)\mathcal{I}_1(\boldsymbol{\theta}_0)^{\frac{1}{2}}\boldsymbol{\delta}, \mathcal{I}_1(\boldsymbol{\theta}_0)),$$

so that

$$\sqrt{n}(\hat{\boldsymbol{\theta}}_n - \boldsymbol{\theta}_0) \xrightarrow{d} \text{MVN}(H_1^{-1}(\boldsymbol{\theta}_0)\mathcal{I}_1(\boldsymbol{\theta}_0)^{\frac{1}{2}}\boldsymbol{\delta}, H_1^{-1}(\boldsymbol{\theta}_0)\mathcal{I}_1(\boldsymbol{\theta}_0)H_1^{-1}(\boldsymbol{\theta}_0))$$

and hence,

$$\begin{aligned} T_n &\xrightarrow{d} \mathbf{Z}^T\mathbf{Z} \text{ where } \mathbf{Z} \sim \text{MVN}(\boldsymbol{\delta}, \mathbf{I}_{4\times 4}) \\ &\sim \chi_4^2(\delta_\kappa^2 + \delta_\alpha^2 + \delta_\beta^2 + \delta_\gamma^2). \quad \square \end{aligned}$$

On-line Appendix D: Q-Q plots for Aluminum EBSD Data

Q-Q plots for the fitted misorientation angles obtained from EBSD observations, using the von Mises circular distribution, are presented in Figure D.1 for two sets of aluminum data. The data used here are seven repeat measurements from a single location on the aluminum scans and 50 measurements appearing to be within a single grain from a single scan, respectively. These plots demonstrate that the von Mises distribution appropriately describes the aluminum data. (Figures 2 and 3 of the main manuscript showed goodness-of-fit for nickel EBSD data.)

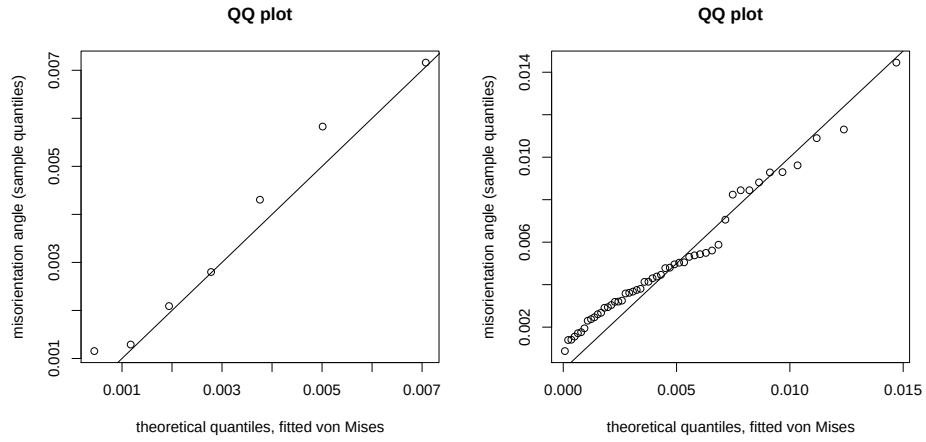

Figure D.1: Q-Q plot for the fitted misorientation angles obtained from two sets of aluminum EBSD observations, using the von Mises circular distribution on the misorientation angle